[American Journal of Science, Vol. 317, April, 2017, P. 483–513, DOI 10.2475/04.2017.03]

PLATINUM-GROUP ELEMENT GEOCHEMISTRY OF THE LAYERED INTRUSIONS IN THE EMEISHAN LARGE IGNEOUS PROVINCE, SW CHINA: IMPLICATIONS FOR THE PRINCIPAL CONTROLS ON MAGMATIC SULFIDE IMMISCIBILITY

YU-WEI SHE*,**, XIE-YAN SONG **,†, LIE-MENG CHEN**, SONG-YUE YU**, XIANG-KUN ZHU*, JUN-NIAN YI**, and JUN-HAO HU**

ABSTRACT. It is widely accepted that the incorporation of external sulfur via crustal contamination is an important trigger for sulfide immiscibility that generates Ni-Cu-(PGE) sulfide mineralization, yet other controlling factors for sulfide immiscibility may also be present. The late Permian Panzhihua, Baima, Hongge, Xinjie and Taihe layered intrusions in the Emeishan Large Igneous Province (ELIP, SW China), are well-endowed with Fe-Ti oxide deposits, whereas their sulfide mineralization is mainly sub-economic. For example, the lower part of the Xinjie intrusion hosts a few thin PGE-rich ore layers, yet other ELIP layered intrusions do not contain any Ni-Cu sulfide mineralization and are PGE-depleted (0.01–1 ppb).

Compared with the PGE-undepleted Emeishan high-Ti basalts that are genetically related to the intrusions, the extent of PGE depletion and elevated Cu/Pd ratios (up to 3.2×10^6) of the Panzhihua, Baima, Taihe and Hongge intrusions suggest PGE-depletion in their parental magmas due to early-stage sulfide removal. Sr-Nd isotopic compositions of the Panzhihua, Baima and Taihe intrusions suggest crustal contamination was insignificant and sulfide saturation produced mainly by crustal sulfur input was unlikely. MELTS modeling shows that extensive fractionation of chromite, olivine and clinopyroxene in deep-seated magma chambers may have induced early-stage sulfide saturation of the primary magmas. The relatively high sulfide contents in the Fe-Ti oxide layers at Panzhihua, Baima, Hongge and Taihe indicate a close relationship between the second-stage sulfide immiscibility and extensive Fe-Ti oxide crystallization.

Positive correlations between sulfur and total Fe_2O_3, V and TiO_2 suggest that Fe-Ti oxide (magnetite and ilmenite) crystallization may have triggered the second-stage sulfide saturation via sharply lowering the Fe concentration and oxygen fugacity of the magmas. Moderate degree of crustal contamination for the Xinjie Fe-Ti oxide-barren rocks may have induced sulfide saturation and accumulation at the lower part of the intrusion. Our calculations indicate that the Xinjie PGE-rich rocks have high R-factors (1000–10000), which are ascribed to PGE-upgrading of the sulfides via reaction with new replenishments of PGE-undepleted magmas. A few Panzhihua, Baima and Taihe samples that contain higher PGE concentrations suggest that the early-stage sulfide droplets at depths were entrained in later magma pulses delivered to shallower magma chambers. The very high R-factors determined by mass balance calculation, implies a good potential for discovering more PGE mineralization in the deep-seated intrusions of the magma plumbing system.

Keywords: Platinum-group elements (PGE), sulfide segregation, crustal contamination, fractional crystallization, Fe-Ti oxides, layered intrusion, Emeishan Large Igneous Province

INTRODUCTION

Mantle-derived magmas cannot easily achieve sulfide saturation during their ascent because sulfur solubility increases with decreasing pressure (Wendlandt, 1982;

* Laboratory of Isotope Geology, Ministry of Land and Resources, Institute of Geology, Chinese Academy of Geological Sciences, Beijing 100037, PR China

** State Key Laboratory of Ore Deposit Geochemistry, Institute of Geochemistry, Chinese Academy of Sciences, Guiyang 550002, PR China

† Corresponding author: E-mail: songxieyan@vip.gyig.ac.cn

Mavrogenes and O'Neill, 1999; Moretti and Baker, 2008; Mungall and Brenan, 2014). In the past several decades, extensive debate has developed over the relative importance of magmatic differentiation, oxygen fugacity, and crustal sulfur input to magmatic sulfide immiscibility (Haughton and others, 1974; Wendlandt, 1982; Mavragenes and O'Neill, 1999; Ripley and Li, 2003; Lightfoot and Keays, 2005; Ripley and others, 2010; Jenner and others, 2010). Platinum-group elements (PGE) are very sensitive to sulfide saturation of mantle-derived magmas because of their extremely high partition coefficients between sulfide and silicate melts (Peach and others, 1990, 1994; Mungall and Brenan, 2014). More than 45 percent and 80 percent of the global Pd and Pt reserves, respectively, are hosted by magmatic sulfide reefs in layered intrusions, notably the Bushveld Complex (South Africa), Great Dyke (Zimbabwe) and Stillwater Complex (US) (Mungall and Naldrett, 2008; Barnes and Ripley, 2016). Crustal contamination is considered to be an important trigger for sulfide saturation, which facilitates the segregation and accumulation of PGE-reef-style mineralization in the Bushveld and Stillwater complexes (Barnes, 1989; Maier and others, 2000, 2008; Ihlenfeld and Keays, 2011; Keays and others, 2012). In some intrusions with smaller and sub-economic PGE mineralization, the PGE reef formation may have been produced by prolonged magmatic fractionation in closed systems with no crustal sulfur input, for example the intrusions at Skaergaard (Greenland), Sonju Lake (Minnesota), Stella (South Africa), Rincon del Tigre (Bolivia) and Rio Jacare (Brazil) (Andersen and others, 1998; Prendergast, 2000; Miller and Andersen, 2002; Maier and others, 2003; Sa and others, 2005; Andersen, 2006; Holwell and Keays, 2014). Extensive magnetite crystallization is suggested to have led to sulfide segregation and PGE enrichment in the Fe-Ti oxide layers of these intrusions (Andersen and others, 1998; Prendergast, 2000; Maier and others, 2003; Holwell and Keays, 2014). Nevertheless, there are also some Fe-Ti oxide layers that are barren of PGE mineralization, as exemplified by the Sept Iles intrusion (Canada) (Namur and others, 2015). Thus, the major controls on sulfide liquid immiscibility and PGE mineralization for layered intrusions remain controversial (Haughton and others, 1974; Wendlandt, 1982; Barnes, 1989; Mavragenes and O'Neill, 1999; Maier and others, 2000, 2008; Ripley and Li, 2003; Lightfoot and Keays, 2005; Ripley and others, 2010; Jenner and others, 2010; Ihlenfeld and Keays, 2011; Keays and others, 2012).

In the central part of the Emeishan Large Igneous Province (ELIP), SW China, several layered intrusions (Panzhihua, Baima, Hongge, Xinjie and Taihe) host world-class Fe-Ti oxide deposits (Panxi Geological Unit, 1984). However, only thin PGE-rich layers (ΣPGE>1300 ppb) have been identified in Cycle I in the lower part of the Xinjie intrusion (Zhong and others, 2011a). The Panzhihua, Baima, Taihe and Hongge intrusions are characterized by PGE depletion compared to the PGE-undepleted Emeishan high-Ti basalts (ΣPGE=10–30 ppb, Zhong and others, 2006; Qi and Zhou, 2008; Song and others, 2009). It has been suggested that the PGE depletion of the layered intrusions may have resulted from the early, deep-level removal of minor sulfides (Zhong and others, 2002; Bai and others, 2012; Zhang and others, 2013; Howarth and Prevec, 2013). The unanswered questions are: (1) why does the Xinjie intrusion contains sub-economic PGE mineralization whereas the other ELIP intrusions are essentially PGE-barren; (2) what major factors triggered sulfide liquid immiscibility at different depths; and (3) what is the potential for economic PGE mineralization in the deep-seated intrusions of the magma plumbing system?

On the basis of a new PGE dataset of the Panzhihua, Hongge and Taihe intrusions and the compilation of recently published major, trace element geochemical and Sr-Nd isotopic data, it is proposed that the sulfide liquid immiscibility in these intrusions was dominantly attributed to extensive Fe-Ti oxide fractionation and crystallization leading to oxygen fugacity changes. Crustal contamination may have

played an important role in sulfide saturation and PGE mineralization in the Xinjie intrusion. The PGE depletions at Panzhihua, Baima, Hongge and Taihe may have been caused by early sulfide removal in their parental magmas, probably led by extensive fractionation of mafic silicates at depth.

GEOLOGICAL BACKGROUND

The ELIP is situated in the western part of the Yangtze Block and eastern margin of the Tibetan Plateau, SW China (Xu and others, 2001; Song and others, 2001, 2004; Ali and others, 2005). The Precambrian metamorphic basement on the western margin of the Yangtze Block is overlain by thick Sinian to lower Permian strata, consisting of clastic, carbonate and meta-volcanic rocks. The Songpan-Ganze Terrane is located in the easternmost part of the Tibetan Plateau, and contains thick (up to ca. 10 km) upper Triassic deep marine strata (Burchfiel and others, 1995).

The ELIP consists mainly of the late Permian Emeishan continental flood basalts that cover at least 5×10^5 km^2 (total volume may be up to 3×10^5 km^3), and the cogenetic mafic-ultramafic and syenitic-granitic intrusions (Xu and others, 2001; Song and others, 2004, 2008; Ali and others, 2005). The Emeishan flood basalts comprise a high-Ti and low-Ti series (Xu and others, 2001; Xiao and others, 2004; Kamenetsky and others, 2012). *In situ* zircons from the cogenetic mafic-ultramafic and felsic intrusions have U-Pb dates of ~260 Ma (Zhou and others, 2002, 2005, 2008; Zhong and Zhu, 2006; Xu and others, 2008; Zhong and others, 2011b; She and others, 2014). Previous trace element and Sr-Nd isotopic geochemistry studies indicated that these intrusive and volcanic rocks were derived from a late Permian mantle plume (Chung and Jahn, 1995; Xu and others, 2001 and references therein). The central zone of the ELIP is marked by low-Ti basalts overlain by high-Ti basalts, whereas the outer zone is dominated by high-Ti basalts (Xu and others, 2001, 2004; Xiao and others, 2004; Song and others, 2009). Small mafic-ultramafic intrusions that host magmatic sulfide deposits, for example Limahe, Zhubu, Jinbaoshan and Baimazhai, are common and are considered to be genetically linked to the low-Ti basalts (Zhou and others, 2008; Zhang and others, 2009), whereas the layered intrusions that host giant Fe-Ti-(V) oxide deposits (Panzhihua, Baima, Hongge, Taihe and Xinjie) are believed to be associated with high-Ti basalts (Zhou and others, 2008, 2013; Zhang and others, 2013). These intrusions are distributed along N-S trending regional faults (fig. 1), which are widely accepted to have formed by Emeishan plume activity (He and others, 2003). Such rift structures are believed to have facilitated the development of interconnecting magma conduits, and the strike-slip motion of the faults may have promoted magma emplacement at depth (Lightfoot and Evanms-Lamswood, 2015).

LAYERED INTRUSIONS OF THE CENTRAL ELIP

The Xinjie Intrusion

The NW-SE trending Xinjie mafic-ultramafic layered intrusion is ~7.5 km long and ~1.2 km thick. It is SW-dipping and was emplaced at the base of the Emeishan high-Ti flood basalts. Xinjie is divided into three cycles from the bottom to the top, namely: Cycle I, II and III (fig. 2) (Zhong and others, 2004, 2011a). Cycle I, capped by a gabbro layer, contains several sub-cycles dominated by peridotite and clinopyroxenite. Cycle II consists of plagioclase-bearing peridotite and olivine clinopyroxenite, gabbro and magnetitite. Cycle III comprises clinopyroxenite overlain by gabbro. Four PGE-rich layers (ΣPGE>1300 ppb; 3–5 meters thick) have been identified within the peridotites in the lower half of the Cycle I (Zhong and others, 2011a). The Xinjie parental magma is considered to share a common mantle source with the nearby high-Ti basalts (Zhong and others, 2004, 2011a). The PGE-rich layers commonly contain < 1 percent sulfides, up to 2 percent locally. The sparsely disseminated sulfides

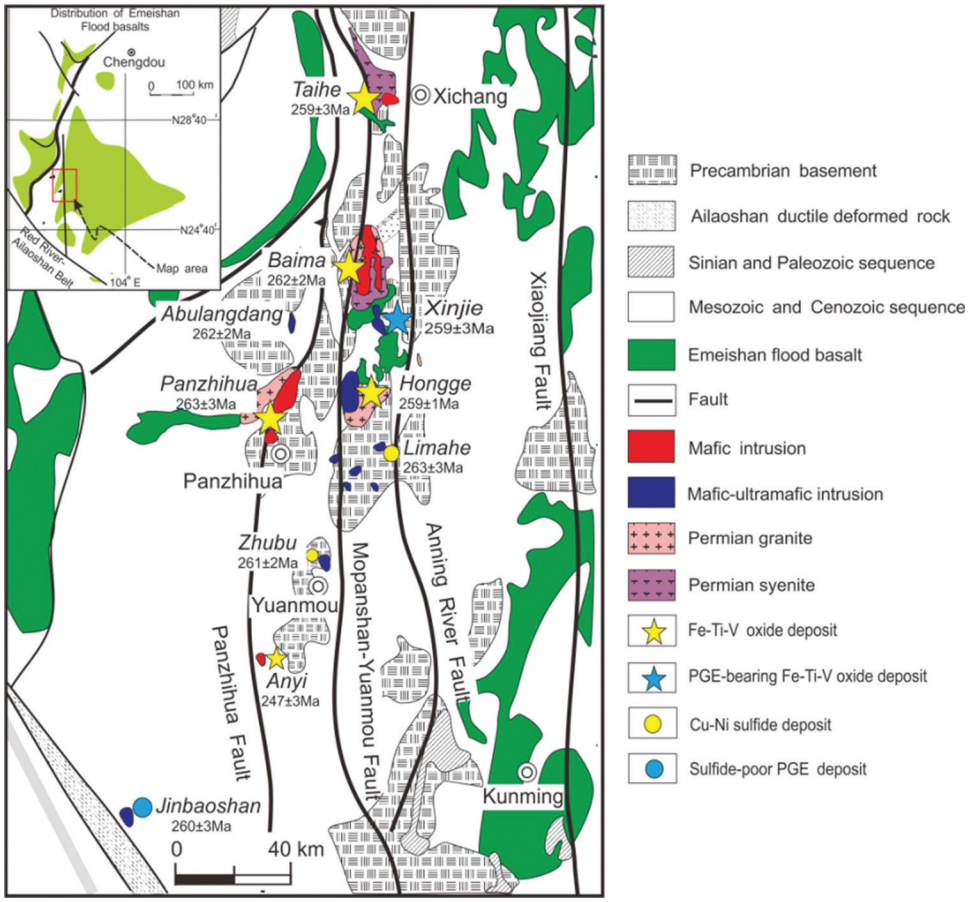

Fig. 1. Simplified geological map of the central ELIP, SW China (Modified after Song and others, 2009), showing the locations of mafic-ultramafic intrusions. Aga data are after Zhou and others (2002, 2005, 2008), Zhong and Zhu (2006), Tao and others (2009), Wang and others (2014), Yu and others (2014) and She and others (2014).

occur as interstitial phases among silicate minerals, and include mainly pyrrhotite, pentlandite and chalcopyrite. Platinum-group minerals, such as sperrylite and Pd-Pt-Bi-Te minerals, are rare and coexist with the base-metal sulfides (Zhu and others, 2010).

The Panzhihua Intrusion

The NE-SW trending Panzhihua intrusion is ~19 km long and ~1.5 km thick, and was emplaced into Neoproterozoic dolomitic limestone, gneiss and schist. The intrusion can be divided into the lower zone (LZ), middle zone (MZ) and upper zone (UZ) from the bottom upwards (fig. 2) (Zhou and others, 2005; Pang and others, 2008; Song and others, 2013). The LZ is characterized by a thick magnetitite layer overlain by magnetite gabbro and gabbro. The MZ comprises mainly alternating magnetite gabbro and gabbro layers, whereas the UZ is marked by the presence of apatite gabbro (Song and others, 2013). In the LZ, the magnetitite contains 2 to 3 percent sulfides (up to 4% locally); the magnetite gabbros and gabbros contain 1 to 2 percent and < 1 percent sulfides, respectively. Sulfide contents of the magnetite gabbro (1–2%) are

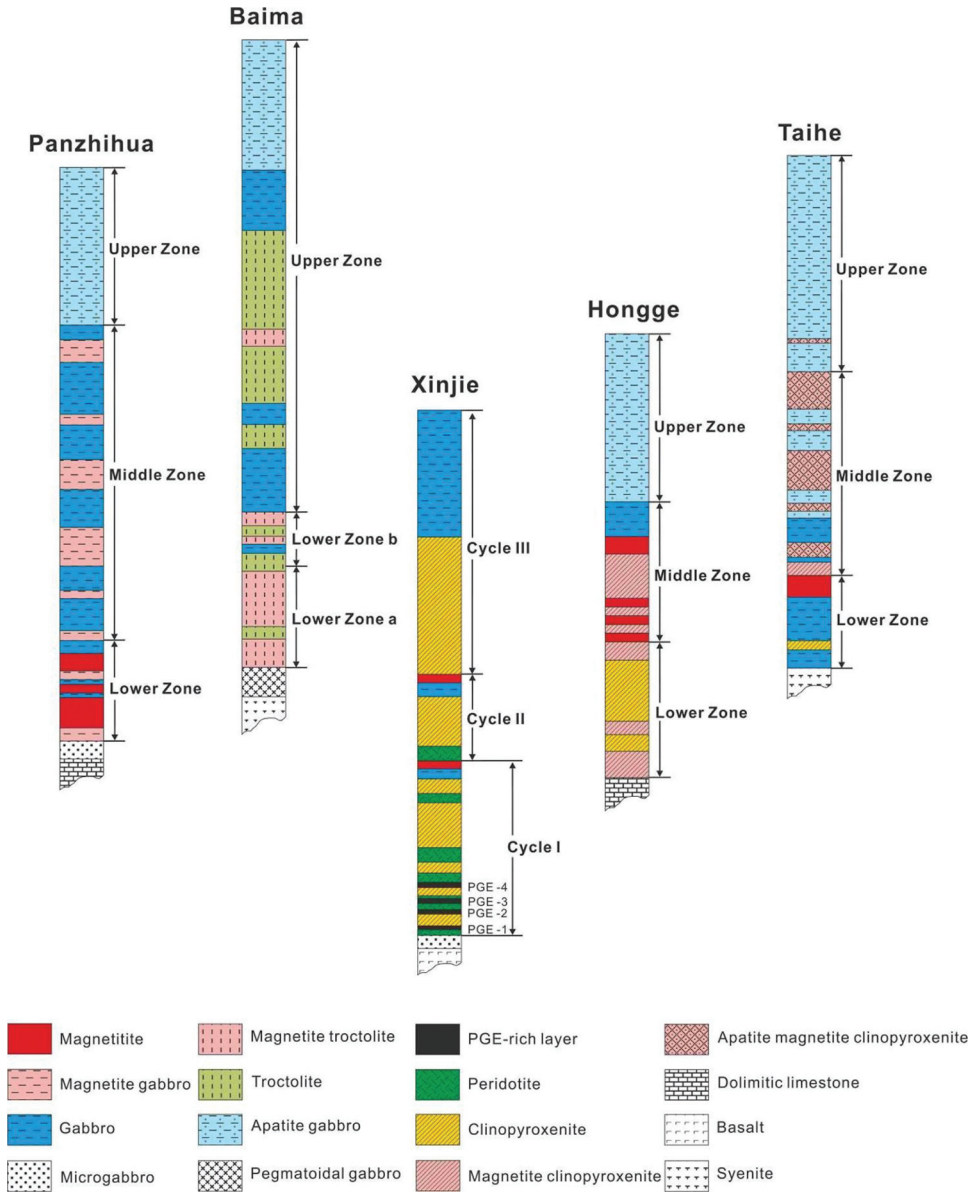

Fig. 2. Petrographic columns of the Panzhihua, Baima, Xinjie, Hongge and Taihe layered intrusions in the central ELIP (Modified after Zhong and others, 2011a; Zhang and others, 2012; Song and others, 2013; Luan and others, 2014; She and others, 2014).

higher than those of the gabbro and apatite gabbro (<1%) in the MZ and UZ, respectively. Overall, the magmatic sulfide abundance correlates positively with the Fe-Ti oxides at Panzhihua. Most of the Panzhihua rocks are PGE-depleted (ΣPGE<1 ppb, Howarth and Prevec, 2013), and are believed to have crystallized from a parental magma similar to those of the Emeishan high-Ti basalts (Zhou and others, 2005; Pang and others, 2008; Song and others, 2013).

The Baima Intrusion

The N-S trending and W-dipping Baima mafic intrusion is ~24 km long and over 2 km thick, and is emplaced into Sinian meta-sandstone, phyllite, slate and marble. The intrusion is surrounded by slightly later syenitic intrusions and cut by syenitic dikes. Zhang and others (2012) and Liu and others (2014) divided the Baima intrusion into a lower zone (LZ) and an upper zone (UZ) (fig. 2). The LZ is further subdivided into LZa comprising magnetite troctolite and troctolite and LZb comprising magnetite troctolite, troctolite and gabbro interlayers. Capped by apatite gabbro, the UZ is mainly composed of gabbro, troctolite and thin interlayers of magnetite troctolite (Zhang and others, 2012). Like the Panzhihua intrusion, sulfide abundance in the Baima intrusive rocks also correlates positively with the Fe-Ti oxide contents. Most magnetite troctolite of the LZa have 1 to 3 percent sulfides, which are closely associated with the Fe-Ti oxide. The LZb magnetite troctolite contains 1 to 2 percent sulfides, whereas the LZb troctolite and gabbro contain much less sulfides (<1%) than the other Fe-Ti oxide-rich rocks. The sulfides contents are much lower than 1 percent in the UZ apatite gabbros and troctolite. Like the Panzhihua rocks, sulfide abundance in the Baima rocks also correlates positively with the Fe-Ti oxide contents. Zhang and others (2013) indicated that the Baima intrusion is PGE-depleted (ΣPGE<1 ppb), and its parental magma likely has similar composition as that of the Emeishan high-Ti basalt.

The Hongge Intrusion

The Hongge intrusion, ~16 km long and ~1.5 km thick, is a sub-horizontal layered lopolith emplaced into Neoproterozoic dolomitic limestone and meta-sandstone. The Emeishan high-Ti basalts are in contact with the roof of the intrusion in the northeastern part (fig. 1). The Hongge intrusion is divided into the lower zone (LZ), middle zone (MZ) and upper zone (UZ) from the base upwards (fig. 2) (Zhong and others, 2002; Bai and others, 2012a; Luan and others, 2014). The LZ is mainly composed of clinopyroxenite with a few magnetite clinopyroxenite interlayers. Capped by gabbro, the MZ consists mainly of thick magnetitite and magnetite clinopyroxenite layers. Apatite gabbro dominates the UZ (Luan and others, 2014). The LZ rocks contain < 1 percent sulfides, whereas the MZ magnetitite and magnetite clinopyroxenite contain 1 to 5 percent sulfides. The MZ and UZ gabbros contain ~1 percent sulfides. The MZ magnetitite and magnetite clinopyroxenite contain lower PGE concentrations (ΣPGE=0.09–63.5 ppb) than the co-genetic PGE-undepleted Emeishan high-Ti basalts (Bai and others, 2012a, 2012b).

The Taihe Intrusion

The Taihe intrusion is ~3 km long and ~1.3 km thick. The intrusion dips to the southeast (dip angles of 50–60°) and is completely surrounded by syenite. Taihe can be divided into the lower zone (LZ), middle zone (MZ) and upper zone (UZ) (fig. 2) (She and others, 2014, 2015). Capped by magnetitite, the LZ is composed chiefly of gabbro with an olivine clinopyroxenite interlayer. The MZ rocks are featured by being apatite- and Fe-Ti oxide-rich, and comprise apatite-magnetite clinopyroxenite and apatite gabbro. The UZ is composed mainly of apatite gabbro and apatite-magnetite clinopyroxenite interlayers. The LZ gabbro and olivine clinopyroxenite contain little sulfides (<1%), whereas the LZ magnetitite contains highly variable sulfide contents (1–3%, up to 4%). In the MZ and UZ, the apatite-magnetite clinopyroxenite contains 1 to 5 percent sulfides, whereas the apatite gabbro contains much lower sulfide contents (<1%). She and others (2016) concluded that the Taihe intrusion is associated with evolution of the high-Ti basaltic magmas.

In conclusion, the rocks in the lower and middle zones of the layered intrusions contain more sulfides than those in the upper zone. Additionally, the sulfides tend to

concentrate along with Fe-Ti oxides (fig. 3). The dominant sulfides in the rocks of the Panzhihua, Baima, Hongge and Taihe intrusions include pyrrhotite, pentlandite and chalcopyrite, which occur as interstitial phases among the cumulus silicates and Fe-Ti oxides (fig. 3). Sulfide blebs are in many places enclosed by magnetite crystals in the magnetitite (fig. 3B). The pyrrhotite commonly displays pentlandite and magnetite exsolutions (fig. 3D).

SAMPLING AND ANALYTICAL METHODS

Samples of the Panzhihua intrusion were collected from the northern open-pit of the Panzhihua mine (Song and others, 2013), and samples of the Hongge and Taihe intrusions were collected from drill cores (Luan and others, 2014; She and others, 2014). All samples (~500–700 grams) were crushed using steel jaws and then milled to 200 mesh.

Platinum-group elements (Ir, Rh, Ru, Pt and Pd) were determined by isotope dilution (ID)-ICP-MS using an improved digestion technique at the State Key Laboratory of Ore Deposit Geochemistry, Institute of Geochemistry, Chinese Academy of Science. The analytical method is reliable and suitable for PGE analyses of mafic-ultramafic rocks. The analytical procedure was described in detail in Qi and others (2011) and summarized below: Ten grams of powdered samples and appropriate amounts of isotope spike solutions enriched in ^{193}Ir, ^{101}Ru, ^{194}Pt and ^{105}Pd were weighed and placed in a PTFE beaker for digesting. Subsequently, the digested samples were used to pre-concentrate PGE by Te-co-precipitation. Last, the Te-precipitates were dissolved with aqua regia and purified through a mixed ion exchange column (a Dowex 50W X8 cation exchange resin and a P507 levextrel resin) for analysis. Iridium, Ru, Pt, and Pd were measured using ICP-MS, whilst Rh was obtained by external calibration using^{194} Pt as an internal standard (Qi and others, 2004).

The detection limits (DL) were calculated as three times the standard deviation of four individual procedural blanks to range from 0.001 ng/g (Ir) to 0.012 ng/g (Pd), and the total procedural blanks of this study vary from 0.001 ng (Rh) to 0.017 ng (Pd) (table 1). Analytical results for the CCRMP (CANMET, Ottawa, Canada) certified reference materials WGB-1, TDB-1 and UMT-1 agree well with the certified values and results reported by Meisel and Moser (2004), Qi and others (2008, 2011) (table 1). Four duplicates were analyzed and the repetition was good (table 1). PGE concentrations of the analyzed Panzhihua, Hongge and Taihe rocks are listed in tables 2, 3 and 4, respectively.

PLATINUM-GROUP ELEMENT CONCENTRATIONS

In the primitive mantle-normalized PGE diagram (fig. 4), the PGE-rich layers and sulfide-bearing rocks of the Xinjie Cycle I are featured by a more variable PGE enrichment relative to the PGE-undepleted Emeishan high-Ti basalts. As for the Panzhihua, Baima and Taihe layered intrusions, some LZ rocks contain similar PGE patterns to the PGE-undepleted high-Ti basalts, whereas most of the MZ and UZ rocks have PGE concentrations comparable to those of the PGE-depleted high-Ti basalts (figs. 4B, 4C, 4E and 4F). It is also notable that some Hongge LZ and MZ rocks show a relatively flat PGE pattern and slightly higher PGE concentrations than that of the PGE-undepleted high-Ti basalts (fig. 4D). A few Taihe MZ and LZ samples show positive Pt anomalies (figs. 4E and 4F).

The layered intrusive rocks exhibit good positive correlations among Pt, Pd, Ir and Rh, although there is some scattering in the Ir data, when Ir concentration is <0.01 ppb (fig. 5). The Xinjie Cycle I rocks have significantly higher PGE concentrations than the samples from the other layered intrusions and the PGE-depleted high-Ti basalts (fig. 5). A few Taihe MZ and LZ samples show no correlation of Pt with Ir and Pd (figs. 5A and 5C). Samples from the Panzhihua, Baima, Hongge and Taihe

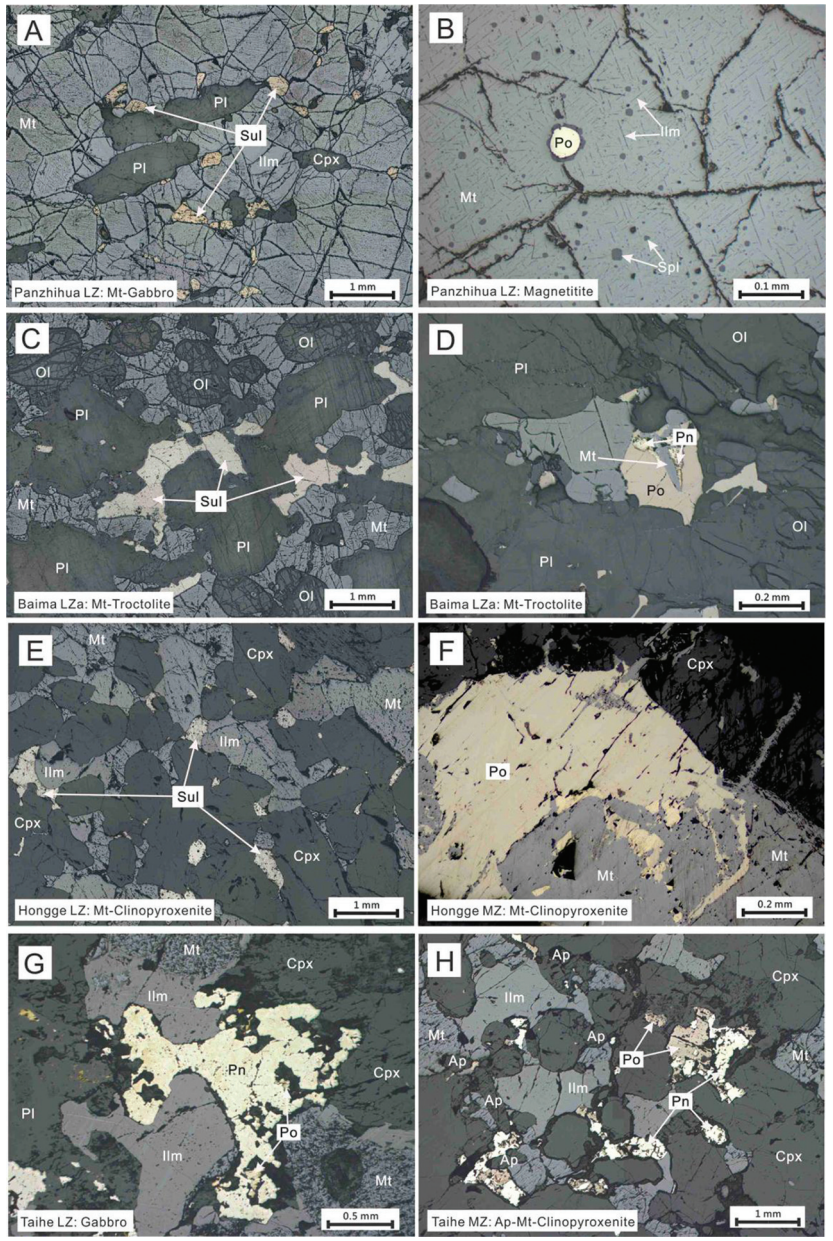

Fig. 3. Photomicrographs of sulfide minerals of the layered intrusions (reflected light). (A) Interstitial sulfides between Fe-Ti oxide and silicate minerals in magnetite gabbro from the Panzhihua Lower Zone. (B) Rounded pyrrhotite enclosed by magnetite in magnetitite from the Panzhihua Lower Zone. (C) Irregular interstitial sulfides between cumulus olivine, plagioclase and Fe-Ti oxide in magnetite troctolite from the Baima Lower Zone a. (D) Pyrrhotite with exsolution of magnetite and pentlandite in magnetite troctolite from the Baima Lower Zone a. (E) Interstitial sulfides between Fe-Ti oxide and silicate minerals in magnetite clinopyroxenite from the Hongge Lower Zone. (F) Pyrrhotite closely associated with magnetite in magnetite clinopyroxenite from the Hongge Middle Zone. (G) Interstitial pentlandite and minor pyrrhotite assemblages in the Taihe Lower Zone gabbro. (H) Interstitial pyrrhotite and pentlandite assemblages between the Fe-Ti oxide and silicate minerals in apatite-magnetite clinopyroxenite from the Taihe Middle Zone. Sul = Sulfides; Po = Pyrrhotite; Pn = Pentlandite; Mt = Magnetite; Ilm = Ilmenite; Spl = Spinel; Ol = Olivine; Pl = Plagioclase; Cpx = Clinopyroxene; Ap = Apatite.

TABLE 1

Blank (ng), detection limits (DL) (ppb) and analytical results (ppb) of reference materials of WGB-1, TDB-1 and UMT-1, and duplicates

Elements	Blank-1 (This study)	Blank-2 (This study)	Blank-3 (This study)	Blank-4 (This study)	Average	DL (3σ)		
Ir	0.004	0.003	0.004	0.004	0.004	0.001		
Ru	0.006	0.005	0.006	0.005	0.005	0.002		
Rh	0.002	0.001	0.001	0.001	0.001	0.001		
Pt	0.015	0.016	0.018	0.015	0.016	0.005		
Pd	0.012	0.016	0.021	0.017	0.017	0.012		
Elements	WGB-1 (This study)	WGB-1 (This study)	WGB-1 (This study)	WGB-1 (This study)	Average	Certified value	Meisel and Moser (2004)	Qi and others (2011)
Ir	0.227	0.217	0.191	0.218	0.213	0.330	0.211	0.27±0.03
Ru	0.144	0.141	0.111	0.137	0.133	0.300	0.144	0.15±0.02
Rh	0.202	0.206	0.169	0.216	0.198	0.320	0.234	0.18±0.02
Pt	4.282	4.26	3.43	5.35	4.330	6.10	6.930	4.95±0.52
Pd	12.193	12.08	10.55	12.24	11.767	13.9	13.900	11.8±0.8
Elements	TDB-1 (This study)	TDB-1 (This study)	TDB-1 (This study)	TDB-1 (This study)	Average	Certified value	Meisel and Moser (2004)	Qi and others (2008)
Ir	0.073	0.058	0.067	0.169	0.092	0.150	0.075	0.082±0.01
Ru	0.248	0.271	0.250	0.278	0.262	0.300	0.198	0.22±0.02
Rh	0.503	0.565	0.463	0.511	0.511	0.700	0.471	0.48±0.03
Pt	4.66	4.54	4.29	5.68	4.79	5.80	5.010	5.23±0.28
Pd	23.34	21.53	21.13	22.9	22.23	22.4	24.300	23.0±1.2
Elements	UMT--1 (This study)	UMT--1 (This study)	UMT--1 (This study)	UMT--1 (This study)	Average	Certified value	Meisel and Moser (2004)	Qi and others (2011)
Ir	7.57	8.02	7.84	7.37	7.70	8.80	8.61	8.23±0.35
Ru	9.86	9.40	8.97	9.05	9.32	10.9	10.1	9.83±0.82
Rh	9.75	8.04	10.7	10.0	9.63	9.50	9.10	8.89±0.6
Pt	135	128	137	130	133	129	146	135±6
Pd	105	105	109	108	107	106	113	108±5
Elements	ST11-18	Duplicate of ST11-18	ST11-35	Duplicate of ST11-35	SP05-8	Duplicate of SP05-8	SH10-28	Duplicate of SH10-28
Ir	0.007	0.007	0.013	0.020	0.132	0.137	0.751	0.858
Ru	0.004	0.016	0.020	0.028	0.250	0.239	2.295	2.545
Rh	0.004	0.005	0.020	0.020	0.228	0.246	0.856	0.638
Pt	0.112	0.111	0.678	0.705	6.461	5.480	9.226	8.580
Pd	0.076	0.097	0.723	0.760	19.9	18.9	4.098	5.220

Referenced data are cited from Qi and others (2008, 2011) and Meisel and Moser (2004); Certified values are from Govindaraju (1994).

TABLE 2

Platinum-group element concentrations of the Panzhihua intrusion

Sample	Depth (m)	Rock	Zone	Ni (ppm)	Ir (ppb)	Ru (ppb)	Rh (ppb)	Pt (ppb)	Pd (ppb)	Cu (ppm)	∑PGE (ppb)	S (ppm)
SP05-01	1335	Magnetite gabbro	Lower Zone	22.6	0.001	0.005	0.002	0.044	0.074	78.0	0.127	6300
SP05-02	1332	Magnetite gabbro	Lower Zone	24.6	0.002	0.007	0.001	0.036	0.105	73.1	0.151	6500
SP05-04	1309	Magnetitite	Lower Zone	21.1	0.001	0.002	0.001	0.045	0.068	69.6	0.119	7300
SP05-07	1255	Magnetitite	Lower Zone	127	0.234	0.258	0.309	7.07	13.3	150	21.1	10000
SP05-08	1245	Magnetitite	Lower Zone	127	0.137	0.239	0.246	5.48	18.9	189	25.0	10300
SP05-09	1240	Magnetite gabbro	Lower Zone	129	0.083	0.107	0.138	5.86	4.66	283	10.9	13700
SP05-10	1226	Gabbro	Lower Zone	27.1	0.013	0.008	0.013	0.522	0.190	54.0	0.745	4000
SP05-13	1212	Magnetite gabbro	Lower Zone	50.2	0.040	0.010	0.040	1.75	1.36	94.9	3.20	5700
SP05-15	1202	Gabbro	Lower Zone	25.5	0.009	0.003	0.007	0.368	0.151	49.8	0.539	4100
SP05-17	1190	Magnetite gabbro	Lower Zone	31.7	0.017	0.013	0.020	1.01	0.880	68.6	1.94	5000
SP05-18	1185	Magnetite gabbro	Lower Zone	29.7	0.019	0.004	0.015	0.845	0.527	61.4	1.41	4900
SP05-19	1180	Magnetitite	Lower Zone	158	0.108	0.129	0.131	3.75	10.7	196	14.8	10300
SP05-20	1150	Magnetitite	Lower Zone	117	0.077	0.106	0.099	2.78	5.44	126	8.50	10900
SP05-22	1125	Gabbro	Lower Zone	42.9	0.008	0.005	0.007	0.366	0.176	32.2	0.562	4200
SP05-23	1105	Magnetite gabbro	Middle Zone	25.1	0.021	0.031	0.025	0.814	0.661	55.5	1.55	3496
SP05-24	1075	Gabbro	Middle Zone	21.3	0.013	0.005	0.009	0.537	0.202	47.8	0.766	4994
SP05-25	1055	Gabbro	Middle Zone	16.7	0.010	0.006	0.008	0.402	0.170	38.1	0.596	*3600*
SP05-26	1005	Magnetite gabbro	Middle Zone	49.1	0.042	0.031	0.047	1.62	0.978	69.9	2.72	4395
SP05-27	985	Gabbro	Middle Zone	12.6	0.003	0.006	0.003	0.174	0.120	34.1	0.307	3995
SP05-28	940	Magnetite gabbro	Middle Zone	10.1	0.013	0.005	0.009	0.454	0.308	38.3	0.789	3796
SP05-31	850	Magnetite gabbro	Middle Zone	51.6	0.002	0.005	0.002	0.110	0.176	43.0	0.295	4495
SP05-32	835	Gabbro	Middle Zone	4.21	0.003	0.003	0.003	0.091	0.127	31.7	0.228	3296
SP05-33	795	Gabbro	Middle Zone	7.09	0.002	0.001	0.002	0.101	0.094	25.1	0.200	2497
SP05-35	725	Magnetite gabbro	Middle Zone	3.53	0.001	0.000	0.003	0.097	0.200	36.2	0.302	3196
SP05-36	705	Magnetite gabbro	Middle Zone	8.63	0.001	0.004	0.004	0.172	0.171	43.7	0.351	4395
SP05-37	685	Gabbro	Middle Zone	4.82	0.002	0.008	0.001	0.067	0.070	23.6	0.149	2597

TABLE 3

Platinum-group element concentrations of the Hongge intrusion

Sample	Depth (m)	Rock	Zone	Ni (ppm)	Ir (ppb)	Ru (ppb)	Rh (ppb)	Pt (ppb)	Pd (ppb)	Cu (ppm)	∑PGE (ppb)	S (ppm)
SH10-54	70	Apatite gabbro	Upper Zone	19.9	0.005	0.004	0.002	0.059	0.068	54.8	0.138	1800
SH10-64	221	Apatite gabbro	Upper Zone	6.44	0.004	0.010	0.003	0.045	0.066	31.1	0.127	4060
SH10-65	239	Apatite gabbro	Upper Zone	6.66	0.007	0.007	0.004	0.113	0.128	41.2	0.259	4940
SH10-68	297	Apatite gabbro	Upper Zone	4.78	0.003	0.002	0.003	0.048	0.113	33.9	0.168	4620
SH10-69	323	Apatite gabbro	Upper Zone	6.23	0.005	0.007	0.002	0.099	0.073	36.9	0.187	4980
SH10-204	413	Gabbro	Middle Zone	25.3	0.013	0.029	0.004	0.081	0.166	57.3	0.293	1300
SH10-28	443	Magnetitite	Middle Zone	650	0.958	2.54	0.638	8.58	5.22	242	17.9	17320
SH10-26	462	Magnetite clinopyroxenite	Middle Zone	169	0.023	0.041	0.008	0.187	0.262	186	0.522	3300
SH10-24	503	Magnetite clinopyroxenite	Middle Zone	267	0.014	0.024	0.006	0.143	0.185	240	0.372	2640
SH10-20	571	Magnetitite	Middle Zone	1076	0.793	2.54	0.584	5.41	6.79	223	16.1	1160
SH10-72	596	Magnetite clinopyroxenite	Middle Zone	347	0.091	0.097	0.042	1.88	0.755	305	2.87	4640
SH10-111	651	Magnetite clinopyroxenite	Middle Zone	1420	3.36	5.62	3.40	13.9	27.8	1042	54.0	8640
SH10-102	671	Magnetitite	Middle Zone	1060	0.947	1.53	0.623	9.05	5.99	464	18.1	6400
SH10-100	692	Clinopyroxenite	Lower Zone	133	0.092	0.131	0.064	2.52	2.62	120	5.43	2432
SH10-96	735	Olivine clinopyroxenite	Lower Zone	388	0.905	1.28	0.342	15.6	12.9	65.4	31.1	1504
SH10-94	760	Magnetite olivine clinopyroxenite	Lower Zone	337	0.025	0.035	0.005	0.105	0.345	60.7	0.514	400
SH10-91	792	Olivine clinopyroxenite	Lower Zone	766	1.31	2.14	0.497	7.95	7.64	96.2	19.5	3100
SH10-90	810	Clinopyroxenite	Lower Zone	360	0.888	0.915	0.392	9.89	13.2	152	25.3	2568
SH10-85	877	Olivine clinopyroxenite	Lower Zone	596	1.85	0.615	0.982	28.1	13.5	354	45.1	5360
SH10-84	891	Magnetite olivine clinopyroxenite	Lower Zone	630	1.39	2.05	0.359	10.3	12.9	309	27.0	2872
SH10-82	916	Magnetite olivine clinopyroxenite	Lower Zone	656	2.72	1.78	1.20	30.2	23.5	260	59.3	3120
SH10-77	988	Magnetite olivine clinopyroxenite	Lower Zone	747	0.786	1.41	0.424	12.6	10.1	339	25.2	3280
SH10-75	1017	Magnetite olivine clinopyroxenite	Lower Zone	621	0.345	0.722	0.183	3.69	2.93	105	7.86	2040

TABLE 4

Platinum-group element concentrations of the Taihe intrusion

Sample	Depth (m)	Rock	Zone	Ni (ppm)	Ir (ppb)	Ru (ppb)	Rh (ppb)	Pt (ppb)	Pd (ppb)	Cu (ppm)	∑PGE (ppb)	S (ppm)
ST11-58	81	Apatite gabbro	Upper Zone	10.1	0.001	0.006	0.002	0.034	0.149	87.3	0.192	2700
ST11-56	113	Apatite gabbro	Upper Zone	1.31	0.001	0.005	0.001	0.026	0.024	64.6	0.057	2300
ST11-54	146	Apatite gabbro	Upper Zone	1.18	0.001	0.012	0.001	0.070	0.087	50.8	0.172	2000
ST11-51	173	Apatite magnetite clinopyroxenite	Upper Zone	10.0	0.002	0.006	0.002	0.017	0.054	88.0	0.082	7300
ST11-50	185	Apatite gabbro	Upper Zone	2.34	0.009	0.011	0.003	0.033	0.034	25.9	0.091	2100
ST11-48	216	Apatite gabbro	Upper Zone	2.87	0.001	0.013	0.002	0.025	0.064	44.9	0.105	3600
ST11-02	246	Apatite magnetite clinopyroxenite	Middle Zone	2.12	0.007	0.017	0.010	0.066	0.084	102	0.184	6500
ST11-03	270	Apatite magnetite clinopyroxenite	Middle Zone	2.61	0.005	0.002	0.003	0.026	0.071	133	0.107	12900
ST11-05	305	Apatite magnetite clinopyroxenite	Middle Zone	160	0.003	0.013	0.005	0.380	0.239	174	0.640	3500
ST11-06	323	Apatite magnetite clinopyroxenite	Middle Zone	2.62	0.005	0.017	0.013	0.571	0.453	83.0	1.06	5700
ST11-08	363	Apatite gabbro	Middle Zone	1.95	0.008	0.018	0.011	0.124	0.159	66.9	0.320	4600
ST11-09	381	Apatite magnetite clinopyroxenite	Middle Zone	2.02	0.011	0.031	0.013	0.064	0.118	112	0.238	5100
ST11-10	400	Apatite gabbro	Middle Zone	2.33	0.002	0.005	0.001	0.042	0.062	91.8	0.113	3900
ST11-11	415	Apatite gabbro	Middle Zone	15.0	0.006	0.015	0.004	0.262	0.284	161	0.571	15300
ST11-13	443	Apatite magnetite clinopyroxenite	Middle Zone	3.51	0.001	0.004	0.002	0.100	0.087	120	0.195	5200
ST11-14	459	Apatite magnetite clinopyroxenite	Middle Zone	3.58	0.002	0.002	0.004	0.058	0.035	107	0.100	4600
ST11-15	471	Apatite magnetite clinopyroxenite	Middle Zone	17.0	0.006	0.011	0.006	0.111	0.146	139	0.280	5500
ST11-16	490	Apatite magnetite clinopyroxenite	Middle Zone	3.52	0.006	0.014	0.005	0.150	0.150	155	0.325	5400
ST11-17	506	Apatite magnetite clinopyroxenite	Middle Zone	3.93	0.002	0.002	0.003	0.082	0.082	133	0.171	4800
ST11-18	517	Apatite magnetite clinopyroxenite	Middle Zone	4.09	0.007	0.016	0.005	0.111	0.097	165	0.236	6300
ST11-19	534	Apatite gabbro	Middle Zone	8.97	0.005	0.015	0.004	0.114	0.146	167	0.284	6000
ST11-20	558	Gabbro	Middle Zone	6.55	0.009	0.073	0.038	0.261	0.391	81.7	0.772	700
ST11-21	575	Apatite magnetite clinopyroxenite	Middle Zone	36.8	0.001	0.002	0.004	0.174	0.120	227	0.302	4600
ST11-22	589	Gabbro	Middle Zone	45.9	0.007	0.018	0.007	0.424	0.192	240	0.649	5840
ST11-23	602	Gabbro	Middle Zone	40.2	0.004	0.008	0.005	0.523	0.258	169	0.797	3100
ST11-24	616	Gabbro	Middle Zone	49.0	0.018	0.019	0.015	5.49	0.301	190	5.84	5400
ST11-25	629	Gabbro	Middle Zone	44.9	0.049	0.015	0.067	29.6	0.658	165	30.4	5200
ST11-27	653	Apatite magnetite clinopyroxenite	Middle Zone	13.5	0.003	0.007	0.004	0.118	0.093	206	0.226	7900
ST11-28	665	Apatite magnetite clinopyroxenite	Middle Zone	25.7	0.014	0.026	0.009	0.192	0.289	248	0.529	9000

Table 4
(continued)

Sample	Depth (m)	Rock	Zone	Ni (ppm)	Ir (ppb)	Ru (ppb)	Rh (ppb)	Pt (ppb)	Pd (ppb)	Cu (ppm)	∑PGE (ppb)	S (ppm)
ST11-29	677	Apatite magnetite clinopyroxenite	Middle Zone	19.9	0.004	0.004	0.005	0.114	0.123	234	0.249	9700
ST11-30	688	Gabbro	Middle Zone	92.9	0.009	0.002	0.008	4.368	0.171	1100	4.56	4560
ST11-32	689	Magnetite clinopyroxenite	Middle Zone	35.9	0.008	0.023	0.008	0.175	0.185	230	0.399	7400
ST11-33	714	Magnetite clinopyroxenite	Middle Zone	34.8	0.004	0.006	0.004	0.131	0.145	210	0.289	5000
ST11-34	728	Magnetitite	Lower Zone	153	0.020	0.037	0.026	0.772	0.693	871	1.55	14640
ST11-35	744	Magnetitite	Lower Zone	71.3	0.020	0.028	0.020	0.705	0.760	177	1.53	9600
ST11-39	756	Magnetitite	Lower Zone	281	0.009	0.022	0.010	0.291	0.254	307	0.585	1480
ST11-40	765	Magnetitite	Lower Zone	419	0.016	0.004	0.026	1.289	0.842	462	2.18	2600
ST11-41	780	Gabbro	Lower Zone	125	0.179	0.047	0.288	18.718	1.63	269	20.9	2120
ST11-42	804	Olivine gabbro	Lower Zone	168	0.240	0.994	1.09	15.911	59.8	211	78.1	1640
ST11-43	820	Gabbro	Lower Zone	195	0.449	3.991	2.51	20.936	8.11	155	36.0	1800
ST11-44	839	Gabbro	Lower Zone	127	0.016	0.204	0.035	0.515	1.44	165	2.21	1700
ST11-45	854	Gabbro	Lower Zone	206	0.017	0.018	0.057	13.656	1.62	328	15.4	3680
ST11-46	871	Olivine clinopyroxenite	Lower Zone	165	1.16	1.06	0.351	5.799	11.2	128	19.5	2100

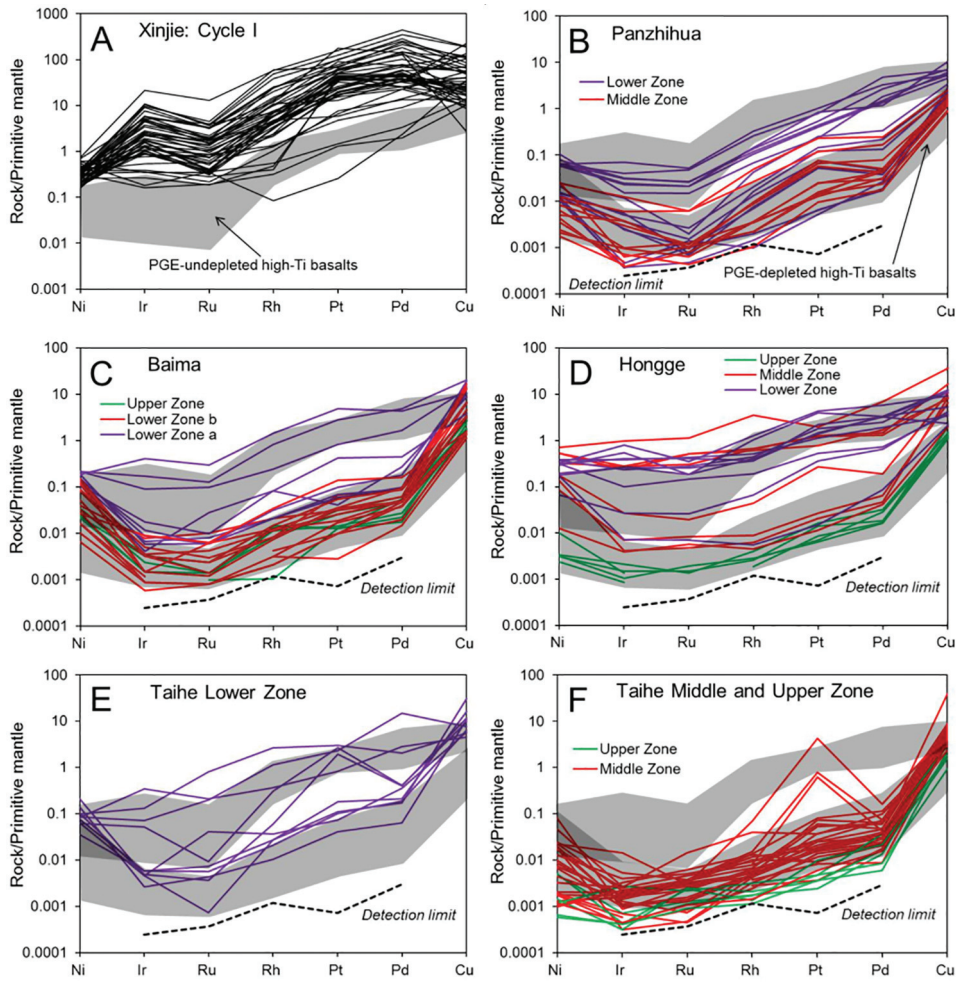

Fig. 4. Primitive mantle-normalized platinum-group element patterns of rocks from the Xinjie, Panzhihua, Baima, Hongge and Taihe intrusions. Normalized values are from Barnes and Maier (1999). The values of the PGE-undepleted high-Ti basalt are from Zhong and others (2006), Qi and Zhou (2008) and Song and others (2009), and the PGE-depleted high-Ti basalts are from Qi and others (2008) in the central ELIP.

intrusions show positive correlations between Ir, Pd and Cr, whereas there is a negative correlation of Ir and Pd with Cr for the Xinjie samples (figs. 6A and 6B). It is also noted that the samples from Panzhihua, Baima and Taihe show a positive Cu/Zr versus Cr correlation, whereas samples from the Hongge MZ and LZ have large variation in Cu/Zr and relatively constant Cr concentrations (fig. 6C). There is also a positive correlation between Cu/Zr and PGE concentrations in the rocks from all the five intrusions (fig. 6D).

The positive correlation is good between S and the metal concentrations (Ir, Pd, Cu and Ni) for the Xinjie Cycle I rocks (fig. 7), yet such positive correlation is relatively weak for the rocks from other intrusions, particularly, for those with relatively high Ni, Ir and Pd concentrations (fig. 7). In the binary plots of total Fe_2O_3, TiO_2 and V against Pd and S, no discernible correlation is present in the Xinjie Cycle I samples (fig. 8).

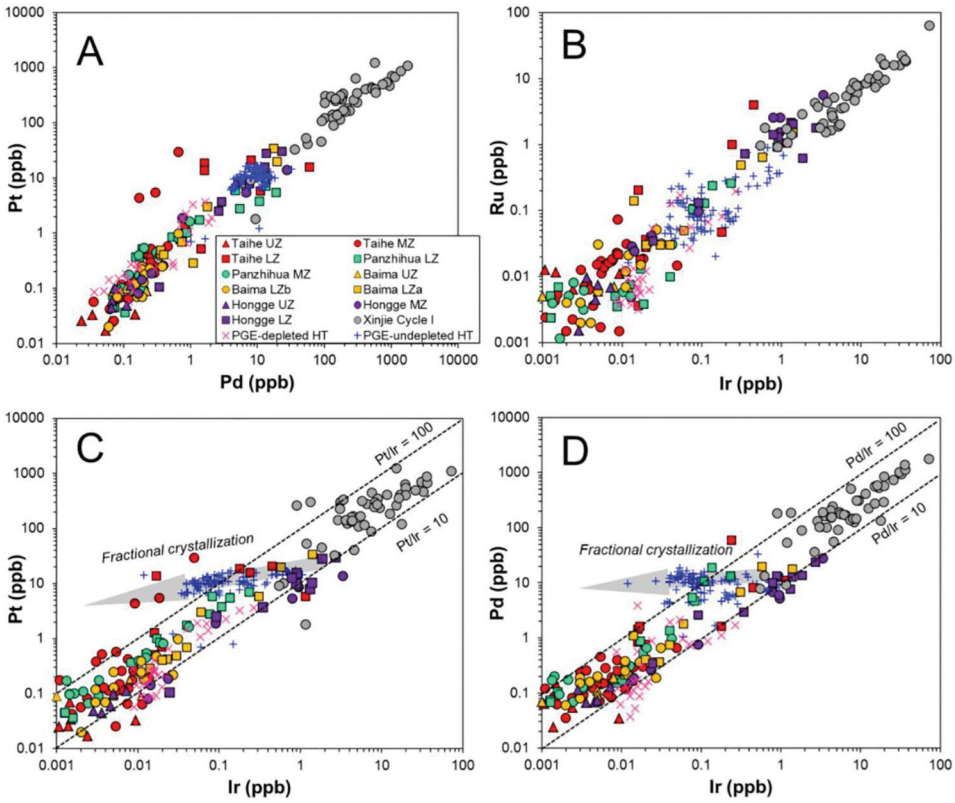

Fig. 5. Binary plots of (A) Pt vs. Pd, (B), (C) and (D) Ru, Pt and Pd vs. Ir of rocks from the Panzhihua, Baima, Xinjie, Hongge and Taihe intrusion, respectively.

Sulfur shows positive correlations with total Fe_2O_3, TiO_2 and V for most of the rocks from Panzhihua, Baima, Hongge and Taihe (figs. 8B, 8D and 8F). Most samples from Panzhihua, Baima and Taihe have their Pd correlated positively with total Fe_2O_3, TiO_2 and V, but not for the Hongge samples (figs. 8A, 8C and 8E).

Most of Xinjie Cycle I samples have Cu/Pd ratios (1.5×10^2-1.1×10^4) lower than or equal to that of the primitive mantle ($\sim10^4$, Barnes and others, 1993) and the PGE-undepleted high-Ti basalts (5.0×10^3-4.5×10^4) (fig. 9). In contrast, most samples from Panzhihua, Baima and Taihe have much higher Cu/Pd (6.7×10^4-3.2×10^6) than that the primitive mantle, and display similar Cu/Pd ratios (4.1×10^4-4.3×10^5) with the PGE-depleted high-Ti basalt (fig. 9). It is also noteworthy that a few samples from the Panzhihua, Baima and Taihe LZs have relatively low Cu/Pd (3.5×10^3-2.3×10^4) (fig. 9). Different from the others intrusions, most of the Hongge MZ and LZ samples have lower Cu/Pd (5.1×10^3-7.7×10^4) than the UZ ones (3.2×10^5-8.1×10^5) (fig. 9).

DISCUSSION

PGE-depleted Parental Magmas and Prior Sulfide Removal

The occurrences of economic or sub-economic PGE-rich magnetitite layers have been documented in the upper parts of the Skaergaard, Rio Jacare and Stalla intrusions (Maier and others, 2003; Sa and others, 2005; Holwell and Keays, 2014).

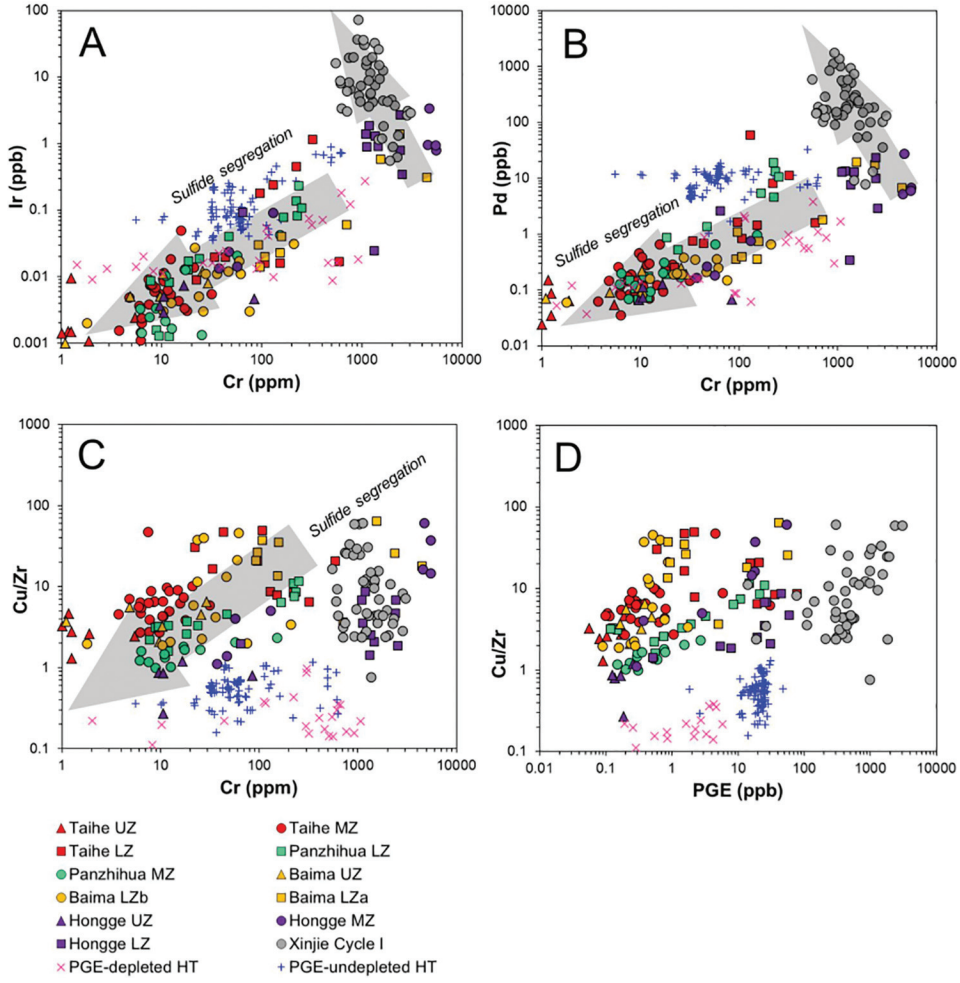

Fig. 6. Binary plots of (A), (B) and (C) Ir, Pd and Cu/Zr vs. Cr, and (D) Cu/Zr vs. PGE of rocks from the Panzhihua, Baima, Xinjie, Hongge and Taihe intrusion, respectively.

PGE enrichment in these intrusions was attributed to sulfide segregation along with magnetite crystallization, led by the prolonged differentiation of an originally PGE-undepleted magma (Andersen and others, 1998; Miller and Andersen, 2002; Maier and others, 2003; Sa and others, 2005; Holwell and Keays, 2014). In the central ELIP, the layered intrusions that host the giant Fe-Ti oxide deposits are co-magmatic with the Emeishan high-Ti basalts, as evidenced by their age, geochemical and isotopic similarities (Zhou and others, 2002, 2008; Zhong and others, 2004; Yu and others, 2015). Due to the fact that PGEs are incorporated preferentially into sulfide liquids (Peach and others, 1990; Mungall and Brenan, 2014) and disseminated sulfides always accumulate with silicates and Fe-Ti oxides in these ELIP layered intrusions (fig. 3), whole-rock PGE concentrations are much higher than PGE concentrations of the magmas, although the cumulus silicates and Fe-Ti oxides are depleted in PGE. Copper and Zr are highly incompatible in silicate minerals and would be concentrated in the residual magma. Zirconium is a lithophile element and Cu is highly chalcophilic, and thus the Cu/Zr

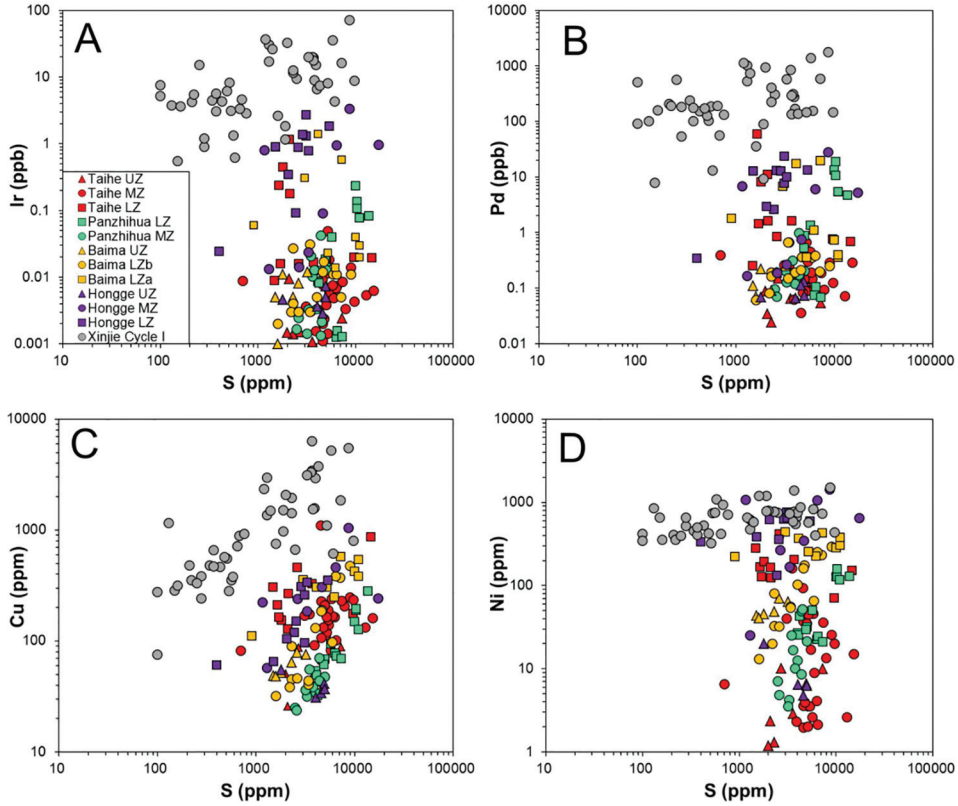

Fig. 7. Binary plots of Ir, Pd, Cu and Ni vs. S concentration of rocks from the Panzhihua, Baima, Xinjie, Hongge and Taihe intrusion, respectively.

ratio serves as a good proxy for chalcophile depletion in the magma (Lightfoot and Hawkesworth, 1997). The positive correlation between Cu/Zr ratio and total PGE concentrations in the layered intrusive rocks indicates that PGE are mainly trapped by sulfides (fig. 6D). However, the Xinjie Cycle I rocks contain much higher PGE than the rocks from the other intrusions, although they have comparable sulfur contents (fig. 7). Particularly, the Xinjie Cycle I rocks not only show higher PGE concentrations than the PGE-undepleted high-Ti basalt but also display PGE enrichment relative to Ni and Cu in the primitive mantle normalized patterns (fig. 4A). This indicates that the sulfides of the Xinjie Cycle I were segregated from a PGE-undepleted parental magma. In contrast, most of the rocks from the other layered intrusions, Panzhihua, Baima, Taihe and Hongge (except for a few samples from the lower zones), are similar to the PGE-depleted high-Ti basalts in PGE concentrations and show PGE depletion relative to Ni and Cu (fig. 4), although the layered intrusion rocks contain minor sulfides (fig. 3). These features indicate that the sulfides in the Panzhihua, Baima, Taihe and Hongge intrusions were segregated from PGE-depleted parental magmas.

The Xinjie Cycle I PGE-rich rocks have Cu/Pd lower than or equal to those of the primitive mantle and the PGE-undepleted high-Ti basalts (Zhong and others, 2006; Qi and Zhou, 2008; Song and others, 2009) (fig. 9). In addition, the Xinjie samples have Cu/Pd value and Pd concentration comparable with the PGE-rich rocks of the Bushveld, Skaergaard, Rio Jacare and Stella intrusions (fig. 9) (Barnes

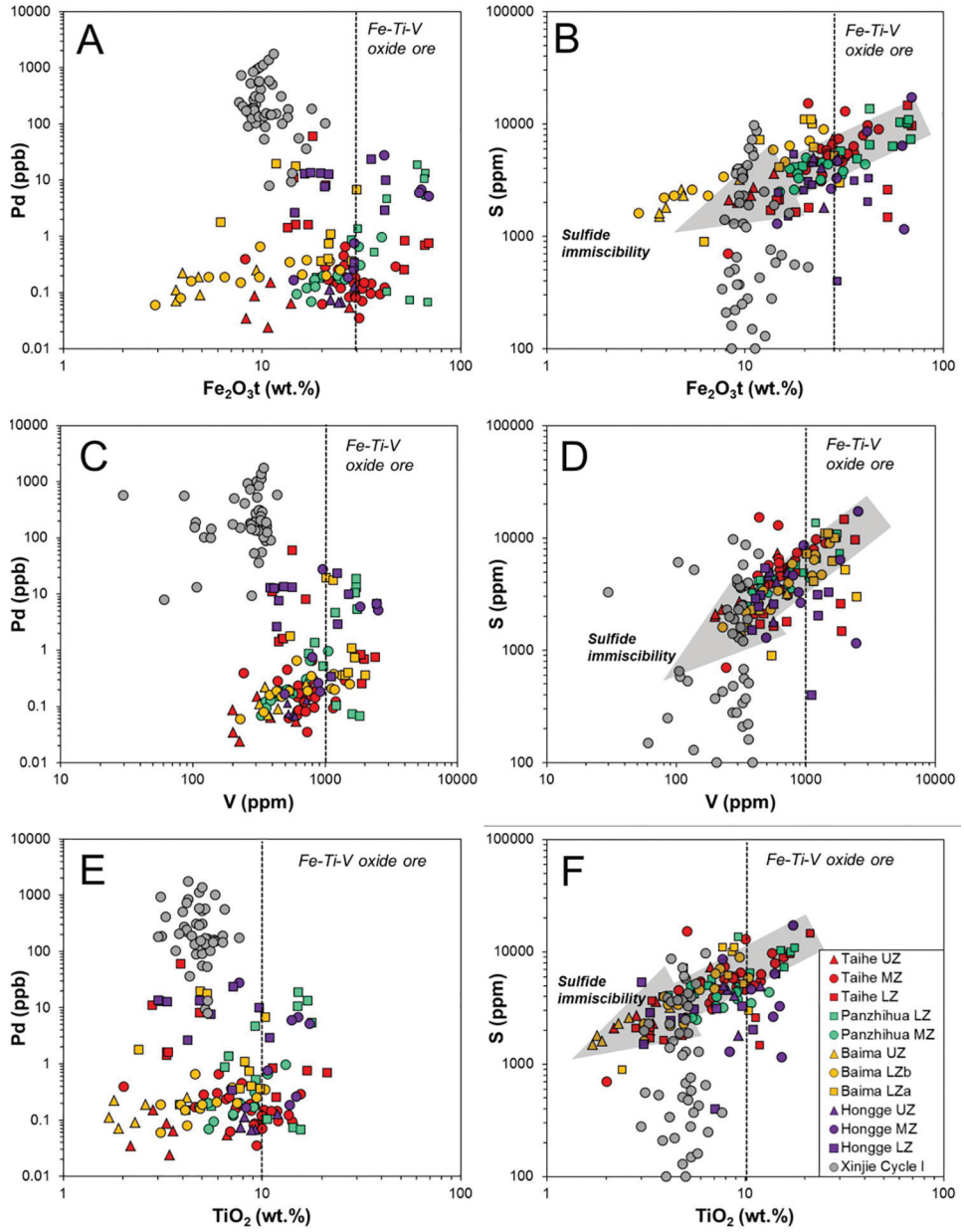

Fig. 8. Binary plots of whole-rock Fe_2O_3 (total), TiO_2 and V vs. Pd and S concentrations of rocks from the Panzhihua, Baima, Xinjie, Hongge and Taihe intrusion, respectively.

and Maier, 2002; Maier and others, 2003; Sa and others, 2005; Ihlenfeld and Keays, 2011; Holwell and Keays, 2014), also indicating that the parental magma of the Xinjie intrusion was sulfide-undersaturated (Zhong and others, 2011a). In contrast, most of the Panzhihua, Baima, Hongge and Taihe rocks have distinctly higher Cu/Pd than the primitive mantle, and are plotted on the same trend as the PGE-depleted high-Ti basalts (Qi and others, 2008) (fig. 9). Qi and others (2008)

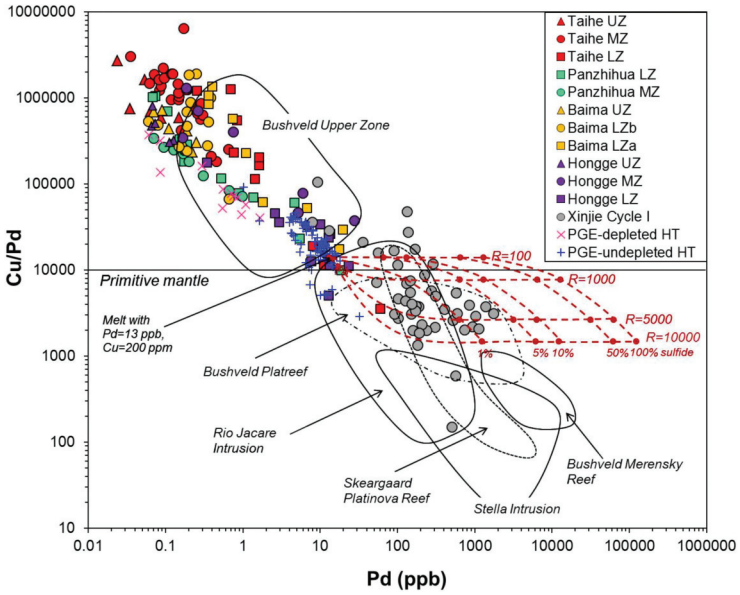

Fig. 9. Plot of Cu/Pd vs. Pd for rocks from the Panzhihua, Baima, Hongge, Taihe and Xinjie intrusions. The red dashed curves which extend from an initial point at 13 ppb Pd and 200 ppm Cu represent the mixing lines between the cumulus phases and sulfides at different R-factors. Sulfide compositions were calculated using the equilibrium fractionation equation (Campbell and Naldrett, 1979) assuming sulfide melt-silicate melt partition coefficients of 1000 for Cu and 200000 for Pd (Peach and others, 1990; Mungall and Brenan, 2014). Fields of other PGE-enriched layered intrusion are from Barnes and Maier (2002), Maier and others (2003), Barnes and others (2004), Sa and others (2005), Ihlenfeld and Keays (2011) and Holwell and Keays (2014).

suggested that the PGE-depleted Emeishan high-Ti basalts may have experienced weak sulfide segregation before the eruption. It is also notable that the Cu/Pd of these ELIP intrusions is similar to or higher than that of the Bushveld Upper Zone PGE-depleted rocks, which was suggested to have formed from the PGE-depleted residual magma due to early sulfide segregation in the lower part of the intrusion (Barnes and others, 2004). Therefore, PGE depletion and high Cu/Pd of the Panzhihua, Baima, Hongge and Taihe intrusions indicate that their parental magmas had undergone prior sulfide removal before their final emplacement.

Cause of Deep-level Sulfide Removal

Experimental studies have shown that sulfur solubility of mafic magmas increases with decreasing pressure and therefore mantle-derived magma could not achieve sulfide saturation itself during ascent (Mavrogenes and O'Neill, 1999; Holzheid and Grove, 2002). Possible mechanisms of sulfide saturation previously proposed include magma mixing, external sulfur input and fractional crystallization (Campbell and others, 1983; Naldrett and others, 1986; Andersen and others, 1998; Barnes and Maier, 2002; Ripley and Li, 2003; Barnes and others, 2008; Keays and Lightfoot, 2010; Holwell and Keays, 2014).

Due to similar solubility of sulfur, mixing of two mafic magmas could not lead to sulfide saturation (Li and Ripley, 2005; Ripley and Li, 2013). Mixing a mafic magma with a felsic magma or addition of SiO_2 is considered to be capable to induce sulfide saturation (Irvine, 1975; Li and Naldrett, 2000; Naldrett and others, 2012). In the ELIP, although large granitoid plutons occur around the layered intrusions, crosscutting

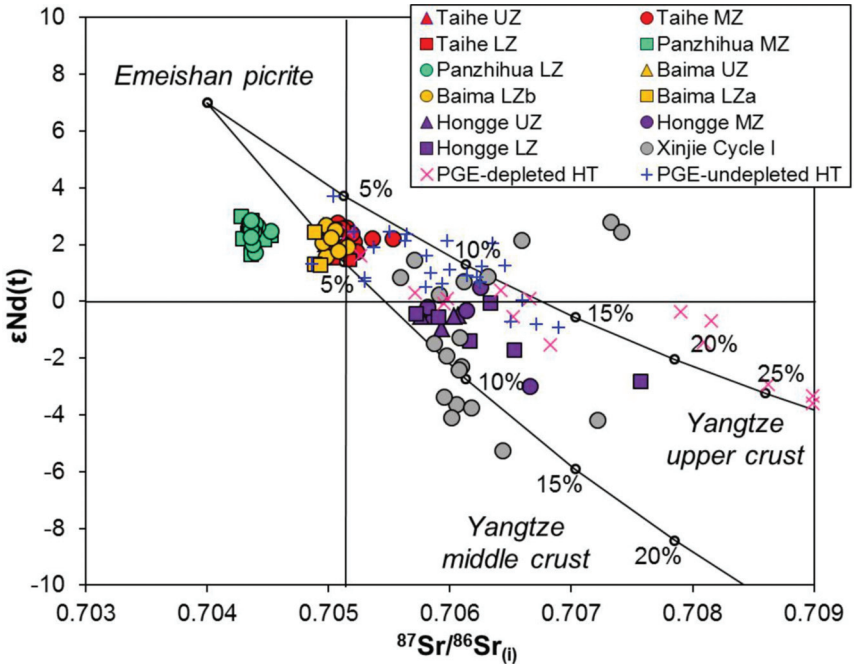

Fig. 10. Binary plot of εNd(t) value vs. $(^{87}Sr/^{86}Sr)_i$ ratio of rocks from the Panzhihua, Baima, Hongge, Xinjie and Taihe intrusions. The calculated parameters of Nd (4.4 ppm), εNd(t) (+7), Sr (102 ppm) and $(^{87}Sr/^{86}Sr)_i$ (0.704) are from picrite in northern Vietnam as primary magma (Wang and others, 2007). The Yangtze upper and middle crust data are from Chen and Jahn (1998). The numbers indicate the percentages of participation of the crustal materials.

relationships suggest that they are younger than the mafic-ultramafic layered intrusions (Xu and others, 2008; Zhong and others, 2011b; Zhang and others, 2012; She and others, 2014). Addition of SiO_2 to mafic magma favors crystallization of orthopyroxene and plagioclase over olivine or clinopyroxene (Irvine, 1970; Sparks, 1986). The ELIP layered intrusions are characterized by the absence of orthopyroxene (Zhong and others, 2002, 2011a; Zhou and others, 2005; Zhang and others, 2012), which suggest that sulfide saturation caused by magma mixing was unlikely.

Incorporation of external sulfur via crustal contamination is considered to be an important sulfide saturation mechanism (Keays, 1995; Ripley and Li, 2003; Keays and Lightfoot, 2007, 2010). Nevertheless, the narrow Sr-Nd isotope variations at Panzhihua, Baima and Taihe suggest that crustal contamination was insignificant (<5%) (fig. 10). This is consistent with the mantle-like $\delta^{18}O$ signature of the magmas in equilibrium with clinopyroxene in the layered intrusions (mean $\delta^{18}O_{melt}$: Panzhihua = 6.1‰, Baima = 5.7‰ and Taihe = 5.9‰) (Yu and others, 2015). In contrast, the Sr-Nd isotopes (εNd_{260}: −2.82 to 0.49; $(^{87}Sr/^{86}Sr)_i$: 0.7057 to 0.7076) and oxygen isotope ($\delta^{18}O_{melt}$: 5.8 to 7.1‰) for the Hongge rocks indicate a slightly higher degree of crustal contamination (Luan and others, 2014; Yu and others, 2015) (fig. 10), which may have induced the sulfide saturation.

Sulfur is strongly incompatible with silicates and oxides, and extensive fractional crystallization could result in sulfur enrichment in the residual magma and eventually sulfide saturation. In sulfide-undersaturated magma, elements for example Cr, Ni, Ir, Ru, Rh and Pt are likely to be partitioned into chromite, olivine and pyroxene, whereas Cu, S and Pd are likely to remain in the residual magma (Duke, 1976; Peach and

others, 1990, 1994; Hauri and others, 1994; Crocket and others, 1997; Righter and others, 2004 and references therein). The PGE mineralization in the upper parts of the Skaergaard, Sonju Lake, Stella, Rincon del Tigre and Rio Jacare intrusions is suggested to have resulted from weak sulfide segregation triggered by prolonged fractionation of mafic magma, as demonstrated by the relatively small amount of sulfides (<0.5%), which are richer in Cu and Pd than Ni and Pt (Andersen and others, 1998; Prendergast, 2000; Maier and others, 2003; Sa and others, 2005; Holwell and Keays, 2014). The forsterite content (Fo value) of olivine in the Panzhihua (Fo_{61-81}), Baima (Fo_{55-75}), Hongge (Fo_{72-82}) and Taihe (Fo_{62-75}) rocks are markedly lower than that of the olivine phenocrysts (Fo_{88-92}) of the Emeishan high-Ti picrites (Pang and others, 2009; Zhang and others, 2011, 2012; Bai and others, 2012a; She and others, 2014; Zhang and others, 2006; Kamenetsky and others, 2012). This observation indicates that the parental magmas may have experienced extensive fractional crystallization before entering the layered intrusions (Pang and others, 2009; Song and others, 2013 and references therein). Furthermore, in sulfide-saturated magma, PGE, Cu and Ni are preferentially concentrated in the sulfide liquid (Peach and others, 1990, 1994; Crocket and others, 1997). Yttrium is incompatible with all silicates and oxides and sulfide liquid, whereas Cr is compatible with mafic silicates and oxides (Hauri and others, 1994; Nielsen and others, 1992; Bindeman and others, 1998; Klemme and others, 2006). Fractionation of olivine, clinopyroxene and chromite from mafic magma would increase Y/Cr and decrease Pd/Y. In contrast, the removal of sulfide liquids resulting from external sulfur addition would decrease Pd/Y without changing Y/Cr. Thus, the negative Pd/Y versus Y/Cr correlation for the Panzhihua, Baima, Taihe and Hongge samples suggests that the deep-level sulfide saturation and segregation were mainly attributed to fractionation of mafic silicates and chromite (fig. 11).

The sulfur content at sulfide saturation (SCSS) in the magma is mainly controlled by temperature, pressure and magma compositions (Mavrogenes and O'Neill, 1999; Li and Ripley, 2005, 2009). Using the melt inclusion composition in the Emeishan high-Ti picrite olivine phenocryst (Fo=88, Kamenetsky and others, 2012) as a starting composition, the MELTS modeling indicates that the sulfur content in the evolving magma increases with fractional crystallization of spinel, olivine, and clinopyroxene (fig. 12). According to the equation of Li and Ripley (2009), SCSS decreases progressively with fractional crystallization of the primary magma (fig. 12). Calculation shows that sulfide saturation in the evolving magma is achieved by 43 percent fractionation of spinel, olivine and clinopyroxene in the deep crust if no external sulfur is involved (fig. 12). It is also noticed that the Hongge rocks have relatively low εNd_t and $(^{87}Sr/^{86}Sr)_I$, indicating a modest degree of crustal contamination (fig. 10). Luan and others (2014) and Yu and others (2015) suggested that the parental magma of the Hongge intrusion were most likely contaminated by the footwall meta-sandstone. Therefore, prior sulfide removal at depth before the magma entered the Hongge intrusion probably resulted from fractionation of mafic minerals.

Second-stage Sulfide Saturation in the Layered Intrusions

Experiments and theoretical calculations indicated that Ir is strongly compatible to chromite in sulfide-undersaturated mafic magma, whereas Pd is much less compatible (Barnes and Picard, 1993; Brenan and others, 2003, 2005, 2012; Page and others, 2012). Thus, chromite fractionation may result in differentiation between IPGEs and PPGEs in the magma. If the rocks contain sulfides, PGE concentration would be mostly controlled by the sulfide phases due to the extremely high sulfide/silicate partition coefficients (Peach and others, 1990, 1994; Crocket and others, 1997; Barnes and others, 2006; Mungall and Brenan, 2014). As shown in figure 5, there are good positive correlations of Ir with Ru, Pt and Pd in the Panzhihua, Baima, Hongge, Taihe and Xinjie rocks, which indicate no differentiation between IPGEs and PPGEs and that

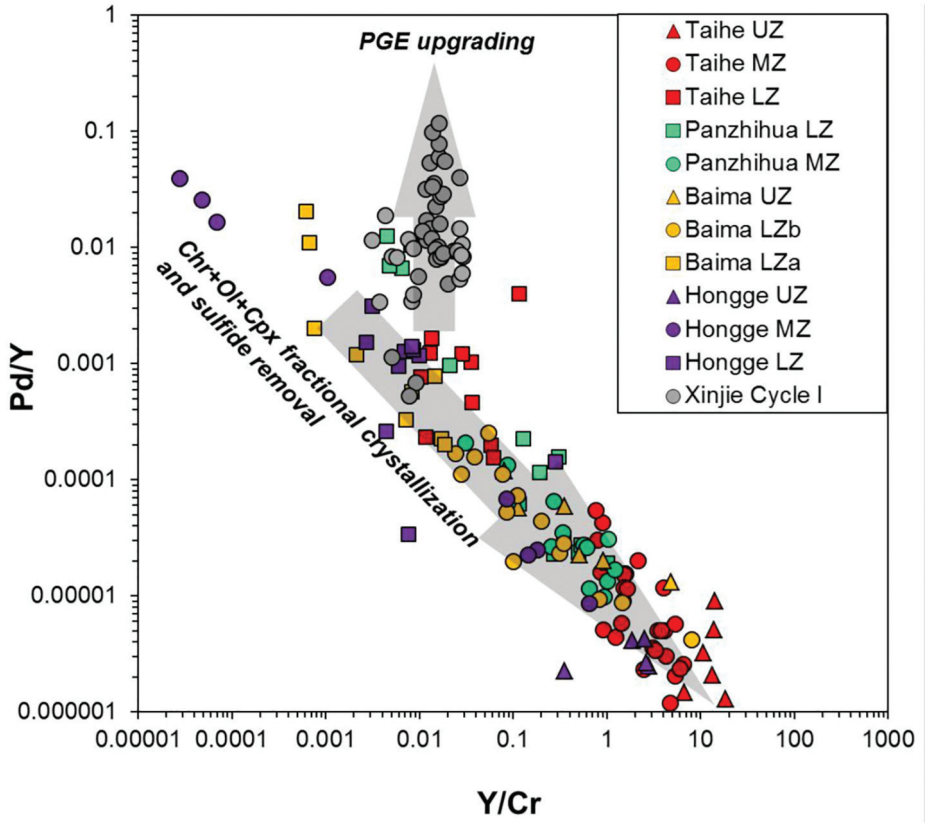

Fig. 11. Plot of Pd/Y vs. Y/Cr ratios of rocks from the Panzhihua, Baima, Xinjie, Hongge and Taihe intrusions.

PGE are mainly hosted by sulfides. Thus, Ir, Pd, Cu and Ni in each of these ELIP intrusions are broadly positively correlated with S (fig. 7). This is consistent with the occurrences of the sparsely disseminated sulfides in the Panzhihua, Baima, Hongge, Taihe and Xinjie intrusions (fig. 3). The positive correlation of Cr with Pd in the Panzhihua, Baima, Hongge and Taihe intrusive rocks (fig. 6B) indicates that the PGE concentrations are unlikely to be controlled by chromite because Pd is incompatible with chromite (Peach and others, 1990, 1994). The negative correlations of Cr with Ir and Pd in the Xinjie Cycle I rocks (figs. 6A and 6B) may be ascribed to the upgrading of PGE in the sulfides via reaction with PGE-undepleted magmas (Zhong and others, 2011a). Upgrading PGE of the sulfides in the Xinjie Cycle I rocks containing much higher PGE than the rocks of the other ELIP layered intrusions with comparable Cu/Zr ratios and sulfur contents (figs. 6D and 7).

In the Panzhihua, Baima, Hongge and Taihe intrusions, the Fe-Ti oxide-rich layers contain higher sulfide contents (1–3%) than the oxide-poor intrusions (<1%), indicating a close relationship between sulfide segregation and Fe-Ti oxide accumulation (fig. 3), as also evidenced by the positive correlations of S with total Fe_2O_3, TiO_2 and V (figs. 8B, 8D and 8F). Moreover, Pd concentration correlates positively with total Fe_2O_3, TiO_2 and V in most of the Panzhihua, Baima, Hongge and Taihe rocks, also suggesting that sulfide liquid immiscibility and Fe-Ti oxide fractionation is genetically linked (figs. 8A, 8C and 8E).

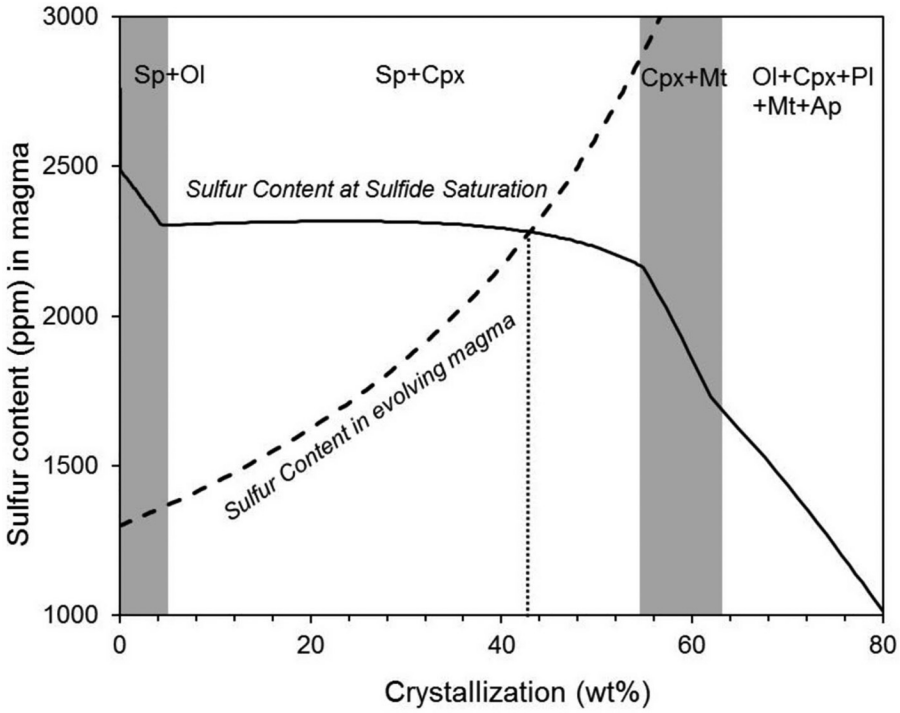

Fig. 12. Variations of sulfur content at sulfide saturation (SCSS) and sulfur content in evolving magma. The melt inclusion data in high-Ti picrite olivine phenocryst (Fo=88) were taken as the starting composition (Kamenetsky and others, 2012). Fractional crystallization was simulated using the MELTS program of Ghiorso and Sack (1995) at 5 kbar and under the assumed oxidation state of FMQ buffer. The SCSS curve is generated using the equation of Li and Ripley (2009). The initial sulfur content in the magma is assumed to be 1300 ppm (Kamenetsky and others, 2012). Ol, olivine; Sp, spinel; Cpx, clinopyroxene; Mt, titanomagnetite; Pl, plagioclase; Ap, apatite.

Experimental studies indicated that sulfur solubility of mafic magma decreases with decreasing Fe^{2+} content and temperature at a constant pressure (Wendlandt, 1982; Mavrogenes and O'Neill, 1999). Crystallization of Fe-Ti oxides significantly reduces the Fe^{2+} content of magma, along with its sulfur carrying capacity that may lead to sulfide immiscibility. In addition, Jugo and others (2005) and Jugo (2009) concluded that small fO_2 changes could strongly affect the sulfur content at sulfide saturation (SCSS). Under reducing conditions ($fO_2 \leq$FMQ), sulfides account for $>$ 95 percent of the total sulfur species in the silicate melt. Sulfate ions (S^{6+}) would be reduced to sulfide ions (S^{2-}) under the sharp fO_2 drop led by magnetite crystallization (Jugo, 2009). This process increases proportionally the S^{2-} in the silicate magma and could trigger sulfide saturation. Consequently, we suggest that the Fe (Fe^{2+} and Fe^{3+}) decreases due to Fe-Ti oxide crystallization may have caused a second-stage sulfide immiscibility in the layered intrusions.

Sulfide droplets and Fe-Ti oxide crystals in the Panzhihua, Baima, Hongge, and Taihe intrusions were precipitated together and accumulated at the Fe-Ti oxide-rich layers of the intrusions. In contrast, in the PGE-rich Xinjie Cycle I rocks, S and Pd do not correlate positively with total Fe_2O_3t, TiO_2 and V (fig. 8), indicating that the sulfide immiscibility was unlikely to be led by Fe-Ti oxide crystallization. This model is consistent with the negative correlations of Ir and Pd with Cr in the Xinjie Cycle I rocks (figs. 6A and 6B). The same conclusion is also reached by the lack of Cu/Zr versus Cr

correlation in the Xinjie rocks (fig. 6C). Zhong and others (2004) showed that the Xinjie Cycle I rocks have relatively low εNd_{260} values (−4.11 to 2.79) and high $(^{87}Sr/^{86}Sr)_i$ ratios (0.7056 to 0.7074) (fig. 10). This indicates that the sulfide saturation associated with the Xinjie Cycle I PGE mineralization was likely to be triggered by variable degrees of crustal contamination.

Sulfide PGE-upgrade and Deep-level PGE Mineralization Potential

The R-factor, as defined by Campbell and Naldrett (1979), is the mass ratio of silicate to sulfide liquids during sulfide saturation. Due to the large partition coefficients of PGE between sulfide and silicate melt, Campbell and Naldrett (1979) emphasized the influence of the high R-factor on the significant PGE mineralization in mafic-ultramafic intrusions. Compositions of the immiscible sulfide liquid could be modeled using the equilibrium fractionation equation (Campbell and Naldrett, 1979):

$$Y_i = X_i^o D_i^{sul/sil}(R+1)/(R+D_i^{sul/sil}) \quad (1)$$

where Xio is the initial concentrationwhere X_i^o is the initial concentration of i in silicate liquid, $D_i^{sul/sil}$ is the partition coefficient of i between silicate and sulfide liquid, and Y_i the is concentration of i in the sulfide liquid, and R is the R-factor. It is assumed that the parental magma of the Xinjie Cycle I rocks is compositionally similar to the Emeishan high-Ti basalt, which contains 13 ppb Pd and 200 ppm Cu (Song and others, 2009). A $D_{Pd}^{sul/sil}$ of 200000 is used for the modeling (Mungall and Brenan, 2014). Calculations show that the PGE-rich Xinjie Cycle I samples are plotted in the 0.5 to 2 percent sulfide (R-factors: 1000 to 10000) field in the Cu/Pd versus Pd diagram (fig. 9). Reaction between sulfide droplets and PGE-undepleted magma is very important for PGE mineralization in layered intrusions (Kerr and Leitch, 2005; Naldrett and others, 2009). The large variations of R-factors (1,000 to 10,000) and the low Cu/Pd ratios (mostly $< 10^4$) in the Xinjie Cycle I rocks indicate metal upgrading of the sulfides via reactions with PGE-undepleted magmas (fig. 9). Moreover, the Pd/Y variation is large under a relatively constant Y/Cr for the Xinjie Cycle I samples (fig. 11), suggesting an increase of PGE concentration in a lowly-fractionated magma. Such high PGE concentrations are ascribed to PGE-undepleted magma replenishments, which reacted with the pre-existing sulfide droplets to upgrade the concentrations of PGE.

Apart from the Xinjie Cycle I PGE-rich layers , economic PGE deposits were also documented in the Jinbaoshan intrusion (260±3 Ma) south of Panzhihua (fig. 1) (Tao and others, 2009). The Jinbaoshan deposit is the largest PGE deposit in China, and contains ~45 tons of Pt + Pd ores with grades of 1 to 5 ppm (locally up to 17 ppm) (Tao and others, 2007). Sub-economic PGE mineralization also occurs on the margins of the Zhubu (261±2 Ma) and Abulangdang (262±2 Ma) intrusions (Zhou and others, 2008; Tang and others, 2013; Wang and others, 2014). All of these PGE-mineralized intrusions in the central ELIP show that the sulfide concentration and PGE mineralization occurred in the ultramafic parts of an open magma chamber (Tao and others, 2007; Tang and others, 2013; Wang and others, 2014). The presence of a periodic magma-plumbing system is also indicated by the rhythmic cycles composed of oxide-rich layers and oxide-barren gabbros at Panzhihua, Baima, Hongge and Taihe (Pang and others, 2009; Zhang and others, 2012; Song and others, 2013; Liu and others, 2014; Luan and others, 2014; She and others, 2016). As discussed above, the early-stage sulfide removal along with mafic silicates and minor chromite fractionation may have occurred in deep-seated magma chambers (fig. 12). The relatively high PGE concentrations at a comparable S content in some of Panzhihua LZ, Baima LZa, Taihe LZ, and Hongge LZ and MZ samples (fig. 7) suggest that the large PGE variation may not be associated with any *in situ* sulfide settling in these intrusions. Holwell and others

(2014) proposed that sulfide saturation may have occurred at depth in the River Valley intrusion of Canada, where the sulfide droplets may have been subsequently entrained into a major pulse of magma and then settled in a staging magma chamber within a conduit system. Similarly, the more PGE-rich Panzhihua LZ, Baima LZa, Taihe LZ, and Hongge LZ and MZ samples may have formed in the early-stage segregation of sulfide droplets at depth, which were then entrained into later magma pulses to be settled in the present sites. A few Taihe MZ and LZ samples show no correlation of Pt with Ir and Pd (fig. 5A and C), and the presence of positive Pt anomalies in primitive mantle-normalized patterns (figs. 4E and 4F). This indicates the crystallization of discrete Pt-rich minerals (for example, sperrylite) from the PGE-rich sulfide droplets, and thus points to a deeper-level PGE mineralization potential. The Xinjie intrusion has ~698 Mt of Fe-Ti oxide ores with grades of ~22 weight percent Fe (Wang and others, 2008), indicating a large volume of magma (compared with ~9 wt% Fe of Emeishan high-Ti basalts). The huge Fe-Ti oxide ore reserves at Panzhihua (~1330 Mt at ~33 wt% Fe), Baima (~1479 Mt at ~27 wt% Fe), Hongge (~4572 Mt at ~26 wt% Fe) and Taihe (~1300 Mt at ~33 wt% Fe) suggest that the deep-seated magma chambers beneath these intrusions must be very large. Mass balance calculation indicates that the magmatic volume at Panzhihua, Baima, Hongge and Taihe are 2.6 to 7.7 times greater than that at Xinjie. Thus, there is potential for discovering PGE mineralization at greater depth (than the present prospecting level) in these central ELIP intrusions.

CONCLUSIONS

Parental magmas of the Panzhihua, Baima, Hongge and Taihe intrusions are PGE-depleted due to early and deep-level sulfide removal from the primary magmas. Extensive fractional crystallization of mafic silicates and chromite may have led to this prior sulfide segregation at deep-seated magma chambers in a periodic magma-plumbing system. Subsequently, the evolved magmas may have entered the shallower Panzhihua, Baima, Hongge and Taihe magma chambers and experienced a second-stage sulfide saturation, which resulted from extensive Fe-Ti oxide crystallization and the consequent decrease in. Crustal contamination may have triggered sulfide saturation for the less evolved and Fe-Ti oxide-barren rocks in the lower part of the Xinjie intrusion. Formation of the Xinjie PGE-rich rocks may have been ascribed to high R-factors and to sulfide PGE-upgrading via reaction with the newly-replenished PGE-undepleted magmas. Potential for more PGE mineralization may lie at deeper level in the central ELIP.

ACKNOWLEDGMENTS

This study was funded by the CAS/SAFEA International Partnership Program for Creative Research Teams (Intraplate Mineralization Research Team: KZZD-EW-TZ-20), the strategic priority research program (B) of the Chinese Academy of Sciences (XDB18000000), the National Key Research and Development Program of China (2016YFC060503), research grant from the State Key Laboratory of Ore Deposit Geochemistry, Chinese Academy of Sciences (SKLODG-ZY125-06) and NSFC (41172090, 41473024). Mr. Yu Wei and Prof. Liang Qi are thanked for their assistance in field sampling and PGE laboratory analysis. We are grateful to the three reviewers, Profs. Peter C. Lightfoot, James Mungall, and Nick Arndt, whose constructive comments have greatly enhanced the manuscript. Prof. Xiang-Kun Zhu and Cenozoic Geoscience Editing & Consultancy are acknowledged for its scientific and language editing service.

REFERENCES

Ali, J. R., Thompson, G. M., Zhou, M.-F., and Song, X.-Y., 2005, Emeishan large igneous province, SW China: Lithos, v. 79, n. 3–4, p. 475–489, https://doi.org/10.1016/j.lithos.2004.09.013

Andersen, J. C. Ø., 2006, Postmagmatic sulfur loss in the Skaergaard intrusion: Implications for the formation of the Platinova Reef: Lithos, v. 92, n. 1–2, p. 198–221, https://doi.org/10.1016/j.lithos.2006.03.033

Andersen, J. C. Ø, Rasmussen, H., Nielsen, T. F. D., and Ronsbo, J. G., 1998, The Triple Group and the Platinova gold and palladium reefs in the Skaergaard Intrusion: Stratigraphic and petrographic relations: Economic Geology, v. 93, n. 4, p. 488–509, https://doi.org/10.2113/gsecongeo.93.4.488

Bai, Z.-J., Zhong, H., Naldrett, A. J., Zhu, W.-G., and Xu, G.-W., 2012a, Whole-rock and mineral composition constraints on the genesis of the giant Hongge Fe-Ti-V oxide deposit in the Emeishan large igneous province, southwest China: Economic Geology, v. 107, n. 3, p. 507–524, https://doi.org/10.2113/econgeo.107.3.507

Bai, Z.-J., Zhong, H., Li, C., Zhu, W.-G., and Xu, G.-W., 2012b, Platinum-group elements in the oxide layers of the Hongge mafic–ultramafic intrusion, Emeishan Large Igneous Province, SW China: Ore Geology Reviews, v. 46, p. 149–161, https://doi.org/10.1016/j.oregeorev.2012.02.007

Barnes, S. J., 1989, Are Bushveld U-type parent magmas boninites or contaminated komatiites: Contributions to Mineralogy and Petrology, v. 101, n. 4, p. 447–457, https://doi.org/10.1007/BF00372218

Barnes, S.-J., and Maier, W. D., 1999, The fractionation of Ni, Cu and the noble metals in silicate and sulfide liquids, *in* Keays, R. R., Lesher, C. M., Lightfoot, P. C., and Farrow, C. E. G., editors, Dynamic processes in magmatic ore deposits and their application to mineral exploration: Geological Association of Canada, Short Course Notes, v. 13, p. 69–106.

——— 2002, Platinum-group elements and microstructures of normal Merensky Reef from Impala platinum mines, Bushveld Complex: Journal of Petrology, v. 43, n. 1, p. 103–128, https://doi.org/10.1093/petrology/43.1.103

Barnes, S.-J., and Picard, C. P., 1993, The behaviour of platinum-group elements during partial melting, crystal fractionation, and sulphide segregation: An example from the Cape Smith Fold Belt, northern Quebec: Geochimica et Cosmochimica Acta, v. 57, n. 1, p. 79–87, https://doi.org/10.1016/0016-7037(93)90470-H

Barnes, S.-J., and Ripley, E. M., 2016, Highly siderophile and strongly chalcophile elements in magmatic ore deposits: Reviews in Mineralogy and Geochemistry, v. 81, p. 725–774, https://doi.org/10.2138/rmg.2016.81.12

Barnes, S.-J., Couture, J. F., Sawyer, E. W., and Bouchaib, C., 1993, Nickel-copper occurrences in the Belleterre-Angliers Belt of the Pontiac Subprovince and the use of Cu-Pd ratios in interpreting platinum-group element distributions: Economic Geology, v. 88, n. 6, p. 1402–1418, https://doi.org/10.2113/gsecongeo.88.6.1402

Barnes, S.-J., Maier, W. D., and Ashwal, L. D., 2004, Platinum-group element distribution in the main zone and upper zone of the Bushveld Complex, South Africa: Chemical Geology, v. 208, n. 1–4, p. 293–317, https://doi.org/10.1016/j.chemgeo.2004.04.018

Barnes, S.-J., Cox, R. A., and Zientek, M. L., 2006, Platinum-group element, gold, silver and base metal distribution in compositionally zoned sulfide droplets from the Medvezky Creek Mine, Noril'sk, Russia: Contributions to Mineralogy and Petrology, v. 152, n. 2, p. 187–200, https://doi.org/10.1007/s00410-006-0100-9

Barnes, S. J., Anderson, J. A. C., Smith, T. R., and Bagas, L., 2008, The Mordor Alkaline Igneous Complex, Central Australia: PGE-enriched disseminated sulfide layers in cumulates from a lamprophyric magma: Mineralium Deposita, v. 43, p. 641–662, https://doi.org/10.1007/s00126-008-0187-1

Bindeman, I. N., Davis, A. M., and Drake, M. J., 1998, Ion microprobe study of plagioclase-basalt partition experiments at natural concentration levels of trace elements: Geochimica et Cosmochimica Acta, v. 62, n. 7, p. 1175–1193, https://doi.org/10.1016/S0016-7037(98)00047-7

Brenan, J. M., McDonough, W. F., and Dalpe, C., 2003, Experimental constraints on the partitioning of rhenium and some platinum-group elements between olivine and silicate melt: Earth and Planetary Science Letters, v. 212, n. 1–2, p. 135–150, https://doi.org/10.1016/S0012-821X(03)00234-6

Brenan, J. M., McDonough, W. F., and Ash, R., 2005, An experimental study of the solubility and partitioning of iridium, osmium and gold between olivine and silicate melt: Earth and Planetary Science Letters, v. 237, n. 3–4, p. 855–872, https://doi.org/10.1016/j.epsl.2005.06.051

Brenan, J. M., Finnigan, C. F., McDonough, W. F., and Homolova, V., 2012, Experimental constraints on the partitioning of Ru, Rh, Ir, Pt and Pd between chromite and silicate melt: The importance of ferric iron: Chemical Geology, v. 302–302, p. 16–32, http://dx.doi.org/10.1016/j.chemgeo.2011.05.015

Burchfiel, B. C., Chen, Z., Liu, Y., and Royden, L. H., 1995, Tectonics of the Longmen Shan and adjacent regions, central China: International Geology Review, v. 37, n. 8, p. 661–735, https://doi.org/10.1080/00206819509465424

Campbell, I. H., and Naldrett, A. J., 1979, The influence of silicate: Sulfide ratios on the geochemistry of magmatic sulfides: Economic Geology, v. 74, n. 6, p. 1503–1506, https://doi.org/10.2113/gsecongeo.74.6.1503

Campbell, I. H., Naldrett, A. J., and Barnes, S. J., 1983, A model for the origin of the platinum-rich sulfide horizons in the Bushveld and Stillwater Complexes: Journal of Petrology, v. 24, n. 2, p. 133–165, https://doi.org/10.1093/petrology/24.2.133

Chen, J. F., and Jahn, B. M., 1998, Crustal evolution of southeastern China: Nd and Sr isotopic evidence: Tectonophysics, v. 284, n. 1–2, p. 101–133, https://doi.org/10.1016/S0040-1951(97)00186-8

Chung, S.-L., and Jahn, B. M., 1995, Plume-lithosphere interaction in generation of the Emeishan flood basalts at the Permian-Triassic boundary: Geology, v. 23, n. 10, p. 889–892, https://doi.org/10.1130/0091-7613(1995)023<0889:PLIIGO>2.3.CO;2

Crocket, J. H., Fleet, M. E., and Stone, W. E., 1997, Implications of composition for experimental partitioning of platinum-group elements and gold between sulfide liquid and basalt melt: The

significance of nickel content: Geochimica et Cosmochimica Acta, v. 61, n. 19, p. 4139–4149, https://doi.org/10.1016/S0016-7037(97)00234-2
Duke, J. M., 1976, Distribution of the period four transition elements among olivine, calcic clinopyroxene and mafic silicate liquid: Experimental results: Journal of Petrology, v. 17, n. 4, p. 499–521, https://doi.org/10.1093/petrology/17.4.499
Ghiorso, M. S., and Sack, R. O., 1995, Chemical mass transfer in magmatic processes. IV. A revised and internally consistent thermodynamic model for the interpolation and extrapolation of liquid-solid equilibria in magmatic systems at elevated temperatures and pressures: Contributions to Mineralogy and Petrology, v. 119, n. 2, p. 197–212, https://doi.org/10.1007/BF00307281
Govindaraju, K., 1994, 1994 Compilation of working values and sample description for 383 geostandards: Geostandards and Geoanalytical Research, v. 18, n. S1, p. 1–158, https://doi.org/10.1046/j.1365-2494.1998.53202081.x-i1
Haughton, D. R., Roeder, P. L., and Skinner, B. J., 1974, Solubility of sulfur in mafic magmas: Economic Geology, v. 69, n. 4, p. 451–467, https://doi.org/10.2113/gsecongeo.69.4.451
Hauri, E. H., Wagner, T. P., and Grove, T. L., 1994, Experimental and natural partitioning of Th, U, Pb and other trace elements between garnet, clinopyroxene and basaltic melts: Chemical Geology, v. 117, n. 1–4, p. 149–166, https://doi.org/10.1016/0009-2541(94)90126-0
He, B., Xu, Y.-G., Chung, S.-L., Xiao, L., and Wang, Y., 2003, Sedimentary evidence for a rapid, kilometer-scale crustal doming prior to the eruption of the Emeishan flood basalts: Earth and Planetary Science Letters, v. 213, n. 3–4, p. 391–405, https://doi.org/10.1016/S0012-821X(03)00323-6
Holwell, D. A., and Keays, R. R., 2014, The formation of low-volume, high-tenor magmatic PGE-Au sulfide mineralization in closed systems: Evidence from precious and base metal geochemistry of the Platinova reef, Skaergaard intrusion, East Greenland: Economic Geology, v. 109, n. 2, p. 387–406, https://doi.org/10.2113/econgeo.109.2.387
Holwell, D. A., Keays, R. R., Firth, E. A., and Findlay, J., 2014, Geochemistry and mineralogy of platinum group element mineralization in the River Valley intrusion, Ontario, Canada: A model for early-stage sulfur saturation and multistage emplacement and the implications for "Contact-Type" Ni-Cu-PGE sulfide mineralization: Economic Geology, v. 109, n. 3, p. 689–712, https://doi.org/10.2113/econgeo.109.3.689
Holzheid, A., and Grove, T. L., 2002, Sulfur saturation limits in silicate melts and their implications for core formation scenarios for terrestrial planets: American Mineralogist, v. 87, n. 2–3, p. 227–237, https://doi.org/10.2138/am-2002-2-304
Howarth, G. H., and Prevec, S. A., 2013, Trace element, PGE, and Sr–Nd isotope geochemistry of the Panzhihua mafic layered intrusion, SW China: Constraints on ore-forming processes and evolution of parent magma at depth in a plumbing-system: Geochimica et Cosmochimica Acta, v. 120, p. 459–478, https://doi.org/10.1016/j.gca.2013.06.019
Ihlenfeld, C., and Keays, R. R., 2011, Crustal contamination and PGE mineralization in the Platreef, Bushveld Complex, South Africa: Evidence for multiple contamination events and transport of magmatic sulfides: Mineralium Deposita, v. 46, n. 7, p. 813–832, https://doi.org/10.1007/s00126-011-0340-0
Irvine, T. N., 1970, Crystallization sequences in the Muskox intrusion and other layered intrusions. I. Olivine-pyroxene-plagioclase relations: Geological Society of South Africa Special Publication 1, p. 441−476.
——— 1975, Crystallization sequences in the Muskox intrusion and other layered intrusions—II. Origin of chromitite layers and similar deposits of other magmatic ores: Geochimica et Cosmochimica Acta, v. 39, n. 6−7, p. 991−1020, https://doi.org/10.1016/0016-7037(75)90043-5
Jenner, F. E., O'Neill, H. St. C., Arculus, R. J., and Mavrogenes, J. A., 2010, The magnetite crisis in the evolution of arc-related magmas and the initial concentration of Au, Ag, and Cu: Journal of Petrology, v. 51, n. 12, p. 2445–2464, https://doi.org/10.1093/petrology/egq063
Jugo, P. J., 2009, Sulfur content at sulfide saturation in oxidized magmas: Geology, v. 37, n. 5, p. 415–418, https://doi.org/10.1130/G25527A.1
Jugo, P. J., Luth, R. W., and Richards, J. P., 2005, An experimental study of the sulfur content in basaltic melts saturated with immiscible sulfide or sulfate liquids at 1300 °C and 1.0 GPa: Journal of Petrology. v. 46, n. 4, p. 783–798, https://doi.org/10.1093/petrology/egh097
Kamenetsky, V. S., Chung, S.-L., Kamenetsky, M. B., and Kuzmin, D. V., 2012, Picrites from the Emeishan Large Igneous Province, SW China: A compositional continuum in primitive magmas and their respective mantle sources: Journal of Petrology, v. 53, n. 10, p. 2095–2113, https://doi.org/10.1093/petrology/egs045
Keays, R. R., 1995, The role of komatiitic and picritic magmatism and S-saturation in the formation of ore deposits: Lithos, v. 34, n. 1–3, p. 1–18, https://doi.org/10.1016/0024-4937(95)90003-9
Keays, R. R., and Lightfoot, P. C., 2007, Siderophile and chalcophile metal variations in Tertiary picrites and basalts from West Greenland with implications for the sulfide saturation history of continental flood basalt magmas: Mineralium Deposita, v. 42, n. 4, p. 319–336, https://doi.org/10.1007/s00126-006-0112-4
——— 2010, Crustal sulfur is required to form magmatic Ni–Cu sulfide deposits: Evidence from chalcophile element signatures of Siberian and Deccan Trap basalts: Mineralium Deposita, v. 45, n. 3, p. 241–257, https://doi.org/10.1007/s00126-009-0271-1
Keays, R. R., Lightfoot, P. C., and Hamlyn, P. R., 2012, Sulfide saturation history of the Stillwater Complex, Montana: Chemostratigraphic variation in platinum group elements: Mineralium Deposita, v. 47, n. 1, p. 151–173, https://doi.org/10.1007/s00126-011-0346-7
Kerr, A., and Leitch, A. M., 2005, Self-destructive sulfide segregation systems and the formation of high-grade

magmatic ore deposits: Economic Geology, v. 100, n. 2, p. 311–332, https://doi.org/10.2113/gsecongeo.100.2.311

Klemme, S., Günther, D., Hametner, K., Prowatke, S., and Zack, T., 2006, The partitioning of trace elements between ilmenite, ulvospinel, armalcolite and silicate melts with implications for the early differentiation of the moon: Chemical Geology, v. 234, n. 3–4, p. 251–263, https://doi.org/10.1016/j.chemgeo.2006.05.005

Li, C., and Naldrett, A. J., 2000, Melting reactions of gneissic inclusions with enclosing magma at Voisey's Bay, Labrador, Canada: Implications with respect to ore genesis: Economic Geology, v. 95, n. 4, p. 801–814.

Li, C., and Ripley, E. M., 2005, Empirical equations to predict the sulfur content of mafic magmas at sulfide saturation and applications to magmatic sulfide deposits: Mineralium Deposita, v. 40, n. 2, p. 218–230, https://doi.org/10.1007/s00126-005-0478-8

——— 2009, Sulfur contents at sulfide–liquid or anhydrite saturation in silicate melts: Empirical equations and example applications: Economic Geology, v. 104, n. 3, p. 405–412, https://doi.org/10.2113/gsecongeo.104.3.405

Lightfoot, P. C., and Evans-Lamswood, D., 2015, Structural controls on the primary distribution of mafic–ultramafic intrusions containing Ni–Cu–Co–(PGE) sulfide mineralization in the roots of large igneous provinces: Ore Geology Reviews, v. 64, p. 354–386, https://doi.org/10.1016/j.oregeorev.2014.07.010

Lightfoot, P. C., and Hawkesworth, C. J., 1997, Flood basalts and magmatic Ni, Cu, and PGE sulfide mineralization: Comparative geochemistry of the Noril'sk (Siberian Traps) and West Greenland sequences, *in* Mahoney, J. J., and Coffin, M. F., editors, Large igneous provinces: Continental, oceanic, and planetary flood volcanism: Washington, D.C., American Geophysical Union, Geophysical Monograph Series, v. 100, p. 357–380, https://doi.org/10.1029/GM100p0357

Lightfoot, P. C., and Keays, R. R., 2005, Siderophile and chalcophile metal variations in flood basalts from the Siberian trap, Noril'sk region: Implications for the origin of the Ni-Cu-PGE sulfide ores: Economic Geology, v. 100, n. 3, p. 439–462, https://doi.org/10.2113/gsecongeo.100.3.439

Liu, P.-P., Zhou, M.-F., Wang, C. Y., Xing, C.-M., and Gao, J.-F., 2014, Open magma chamber processes in the formation of the Permian Baima mafic–ultramafic layered intrusion, SW China: Lithos, v. 184–187, p. 194–208, https://doi.org/10.1016/j.lithos.2013.10.028

Luan, Y., Song, X.-Y., Chen, L.-M., Zheng, W.-Q., Zhang, X.-Q., Yu, S.-Y., She, Y.-W., Tian, X.-L., and Ran, Q.-Y., 2014, Key factors controlling the accumulation of the Fe–Ti oxides in the Hongge layered intrusion in the Emeishan Large Igneous Province, SW China: Ore Geology Reviews, v. 57, p. 518–538, https://doi.org/10.1016/j.oregeorev.2013.08.010

Maier, W. D., Arndt, N. T., and Curl, E. A., 2000, Progressive crustal contamination of the Bushveld Complex: Evidence from Nd isotopic analyses of the cumulate rocks: Contributions to Mineralogy and Petrology, v. 140, n. 3, p. 316–327, https://doi.org/10.1007/s004100000186

Maier, W. D., Barnes, S.-J., Gartz, V., and Andrews, G., 2003, Pt-Pd reefs in magnetitites of the Stella layered intrusion, South Africa: A world of new exploration opportunities for platinum group elements: Geology, v. 31, n. 10, p. 885–888, https://doi.org/10.1130/G19746.1

Maier, W. D., De Klerk, L., Blaine, J., Manyeruke, T., Barnes, S.-J., Stevens, M. V. A., and Mavrogenes, J. A., 2008, Petrogenesis of contact-style PGE mineralization in the northern lobe of the Bushveld Complex: Comparison of data from the farms Rooipoort, Townlands, Drenthe and Nonnenwerth: Mineralium Deposita, v. 43, n. 3, p. 255–280, https://doi.org/10.1007/s00126-007-0145-3

Mavrogenes, J. A., and O'Neill, H. St. C., 1999, The relative effects of pressure, temperature and oxygen fugacity on the solubility of sulfide in mafic magmas: Geochimica et Cosmochimica Acta, v. 63, n. 7–8, p. 1173–1180, https://doi.org/10.1016/S0016-7037(98)00289-0

Meisel, T., and Moser, J., 2004, Reference materials for geochemical PGE analysis: New analytical data for Ru, Rh, Pd, Os, Ir, Pt and Re by isotope dilution ICP-MS in 11 geological reference materials: Chemical Geology, v. 208, n. 1–4, p. 319–338, https://doi.org/10.1016/j.chemgeo.2004.04.019

Miller, J. D. J., and Andersen, J. C. O., 2002, Attributes of Skaergaard-type PGE reefs, *in* Boudreau, A. E., editors, 9th International Platinum Symposium Abstract: Durham, North Carolina, Duke University, p. 305–308.

Moretti, R., and Baker, D. R., 2008, Modeling the interplay of fO_2 and fS_2 along the FeS-silicate melt equilibrium: Chemical Geology, v. 256, n. 3–4, p. 286–298, https://doi.org/10.1016/j.chemgeo.2008.06.055

Mungall, J. E., and Brenan, J. M., 2014, Partitioning of platinum-group elements and Au between sulfide liquid and basalt and the origins of mantle-crust fractionation of the chalcophile elements: Geochimica et Cosmochimica Acta, v. 125, p. 265–289, https://doi.org/10.1016/j.gca.2013.10.002

Mungall, J. E., and Naldrett, A. J., 2008, Ore deposits of the platinum-group elements: Elements, v. 4, n. 4, p. 253–258, https://doi.org/10.2113/GSELEMENTS.4.4.253

Naldrett, A. J., Gasparini, E. C., Barnes, S. J., Von Gruenewaldt, G., and Sharpe, M. R., 1986, The Upper Critical Zone of the Bushveld Complex and the origin of Merensky-type ores: Economic Geology, v. 81, n. 5, p. 1105–1117, https://doi.org/10.2113/gsecongeo.81.5.1105

Naldrett, A. J., Wilson, A., Kinnaird, J., and Chunnett, G., 2009, PGE tenor and metal ratios within and below the Merensky Reef, Bushveld Complex: Implications for its genesis: Journal of Petrology, v. 50, p. 625–659, https://doi.org/10.1093/petrology/egp015

Naldrett, A. J., Wilson, A., Kinnaird, J., Yudovskaya, M., and Chunnett, G., 2012, The origin of chromitites and related PGE mineralization in the Bushveld Complex: new mineralogical and petrological constraints: Mineralium Deposita, v. 47, n. 3, p. 209–232, https://doi.org/10.1007/s00126-011-0366-3

Namur, O., Higgins, M. D., and Vander Auwera, J., 2015, The Sept Iles intrusive suite, Quebec, Canada, *in* Charlier, B., Namur, O., Latypov, R., and Tegner, C., editors, Layered intrusions: Dordrecht, Springer Geology, p. 465–515, https://doi.org/10.1007/978-94-017-9652-1_11

Nielsen, R. L., Gallahan, W. E., and Newberger, F., 1992, Experimentally determined mineral-melt partition coefficients for Sc, Y and REE for olivine, orthopyroxene, pigeonite, magnetite and ilmenite: Contributions to Mineralogy and Petrology, v. 110, n. 4, p. 488–499, https://doi.org/10.1007/BF00344083

Pagé, P., Barnes, S.-J., Bédard, J. H., and Zientek, M. L., 2012, *In situ* determination of Os, Ir, and Ru in chromites formed from komatiite, tholeiite and boninite magmas: Implications for chromite control of Os, Ir and Ru during partial melting and crystal fractionation: Chemical Geology, v. 302–303, p. 3–15, https://doi.org/10.1016/j.chemgeo.2011.06.006

Pang, K.-N., Zhou, M.-F., Lindsley, D., Zhao, D.-G., and Malpas, J., 2008, Origin of Fe–Ti oxide ores in mafic intrusions: Evidence from the Panzhihua Intrusion, SW China: Journal of Petrology, v. 49, n. 2, p. 295–313, https://doi.org/10.1093/petrology/egm082

Pang, K.-N., Li, C., Zhou, M.-F., and Ripley, E. M., 2009, Mineral compositional constraints on petrogenesis and oxide ore genesis of the late Permian Panzhihua layered gabbroic intrusion, SW China: Lithos, v. 110, n. 1–4, p. 199–214, https://doi.org/10.1016/j.lithos.2009.01.007

Pang, K.-N., Zhou, M.-F., Qi, L., Shellnutt, J. G., Wang, C. Y., Zhao, D.-G., 2010, Flood basalt-related Fe-Ti oxide deposits in the Emeishan large igneous province, SW China: Lithos, v. 119, n. 1–2, p. 123–136, https://doi.org/10.1016/j.lithos.2010.06.003

Panxi Geological Unit, 1984, Mineralization and Exploration Forecasting of V–Ti Magnetite Deposits in the Panzhihua–Xichang Region (in Chinese).

Peach, C. L., Mathez, E. A., and Keays, R. R., 1990, Sulfide melt-silicate melt distribution coefficients for noble metals and other chalcophile elements as deduced from MORB: Implications for partial melting: Geochimica et Cosmochimica Acta, v. 54, n. 12, p. 3379–3389, https://doi.org/10.1016/0016-7037(90)90292-S

Peach, C. L., Mathez, E. A., Keays, R. R., and Reeves, S. J., 1994, Experimentally determined sulfide melt-silicate melt partition coefficients for iridium and palladium: Chemical Geology, v. 117, n. 1–4, p. 361–377, https://doi.org/10.1016/0009-2541(94)90138-4

Prendergast, M. D., 2000, Layering and precious metals mineralization in the Rincón del Tigre Complex, Eastern Bolivia: Economic Geology, v. 95, n. 1, p. 113–130, https://doi.org/10.2113/gsecongeo.95.1.113

Qi, L., and Zhou, M.-F., 2008, Platinum-group elemental and Sr-Nd-Os isotopic geochemistry of Permian Emeishan flood basalts in Guizhou Province, SW China: Chemical Geology, v. 248, n. 1–2, p. 83–103, https://doi.org/10.1016/j.chemgeo.2007.11.004

Qi, L., Zhou, M.-F., and Wang, C. Y., 2004, Determination of low concentrations of platinum group elements in geological samples by ID-ICP-MS: Journal of Analytical Atomic Spectrometry, v. 19, p. 1335–1339, https://doi.org/10.1039/b400742e

Qi, L., Wang, C. Y., and Zhou, M.-F., 2008, Controls on the PGE distribution of Permian Emeishan alkaline and peralkaline volcanic rocks in Longzhoushan, Sichuan Province, SW China: Lithos, v. 106, n. 3–4, p. 222–236, https://doi.org/10.1016/j.lithos.2008.07.012

Qi, L., Gao, J.-F., Huang, X.-W., Hu, J., Zhou, M.-F., and Zhong, H., 2011, An improved digestion technique for determination of platinum group elements in geological samples: Journal of Analytical Atomic Spectrometry, v. 26, p. 1900–1904, https://doi.org/10.1039/c1ja10114e

Righter, K., Campbell, A. J., Humayun, M., and Hervig, R. L., 2004, Partitioning of Ru, Rh, Pd, Re, Ir, and Au between Cr-bearing spinel, olivine, pyroxene and silicate melts: Geochimica et Cosmochimic Acta, v. 68, n. 4, p. 867–880, https://doi.org/10.1016/j.gca.2003.07.005

Ripley, E. M., and Li, C., 2003, Sulfur isotope exchange and metal enrichment in the formation of magmatic Cu-Ni-(PGE) deposits: Economic Geology, v. 98, n. 3, p. 635–641, https://doi.org/10.2113/gsecongeo.98.3.635

——— 2013, Sulfide Saturation in Mafic Magmas: Is external sulfur required for magmatic Ni-Cu-(PGE) ore genesis?: Economic Geology, v. 108, n. 1, p. 45–58, https://doi.org/10.2113/econgeo.108.1.45

Ripley, E. M., Li, C., Moore, C. H., and Schmitt, A. K., 2010, Micro-scale S isotope studies of the Kharaelakh intrusion, Noril'sk region, Siberia: Constraints on the genesis of coexisting anhydrite and sulfide minerals: Geochimica et Cosmochimica Acta, v. 74, n. 2, p. 634–644, https://doi.org/10.1016/j.gca.2009.10.003

Sá, J. H. S., Barnes, S.-J., Prichard, H. M., and Fisher, P. C., 2005, The distribution of base metals and platinum-group elements in magnetitite and its host rocks in the Rio Jacaré Intrusion, Northeastern Brazil: Economic Geology, v. 100, n. 2, p. 333–348, https://doi.org/10.2113/gsecongeo.100.2.333

She, Y.-W., Yu, S.-Y., Song, X.-Y., Chen, L.-M., Zheng, W.-Q., and Luan, Y., 2014, The formation of P-rich Fe–Ti oxide ore layers in the Taihe layered intrusion, SW China: Implications for magma-plumbing system process: Ore Geology Reviews, v. 57, p. 539–559, https://doi.org/10.1016/j.oregeorev.2013.07.007

She, Y.-W., Song, X.-Y., Yu, S.-Y., and He, H.-L., 2015, Variations of trace element concentration of magnetite and ilmenite from the Taihe layered intrusion, Emeishan large igneous province, SW China: Implications for magmatic fractionation and origin of Fe-Ti-V oxide ore deposits: Journal of Asian Earth Sciences, v. 113, Part 3, p. 1117–1131, https://doi.org/10.1016/j.jseaes.2015.03.029

She, Y.-W., Song, X.-Y., Yu, S.-Y., Chen, L.-M., and Zheng, W.-Q., 2016, Apatite geochemistry of the Taihe layered intrusion, SW China: Implications for the magmatic differentiation and the origin of apatite-rich Fe-Ti oxide ores: Ore Geology Reviews, v. 78, p. 151–165, https://doi.org/10.1016/j.oregeorev.2016.04.004

Song, X.-Y., Zhou, M.-F., Hou, Z.-Q., Cao, Z.-M., Wang, Y.-L., and Li, Y., 2001, Geochemical constraints on the mantle source of the upper Permian Emeishan continental flood basalts, southwestern China: International Geology Review, v. 43, n. 3, p. 213–225, https://doi.org/10.1080/00206810109465009

Song, X.-Y., Zhou, M.-F., Cao, Z.-M., and Robinson, P. T., 2004, Late Permian rifting of the South China Craton caused by the Emeishan mantle plume: Journal of the Geological Society, v. 161, p. 773–781, https://doi.org/10.1144/0016-764903-135

Song, X.-Y., Qi, H.-W., Robinson, P. T., Zhou, M.-F., Cao, Z.-M., and Chen, L.-M., 2008, Melting of the subcontinental lithospheric mantle by the Emeishan mantle plume; evidence from the basal alkaline

basalts in Dongchuan, Yunnan, Southwestern China: Lithos, v. 100, n. 1–4, p. 93–111, https://doi.org/10.1016/j.lithos.2007.06.023
Song, X.-Y., Keays, R. R., Xiao, L., Qi, H.-W., and Ihlenfeld, C., 2009, Platinum-group element geochemistry of the continental flood basalts in the central Emeishan Large Igneous Province, SW China: Chemical Geology, v. 262, n. 3–4, p. 246–261, https://doi.org/10.1016/j.chemgeo.2009.01.021
Song, X.-Y., Qi, H.-W., Hu, R.-Z., Chen, L.-M., Yu, S.-Y., and Zhang, J.-F., 2013, Formation of thick stratiform Fe-Ti oxide layers in layered intrusion and frequent replenishment of fractionated mafic magma: Evidence from the Panzhihua intrusion, SW China: Geochemistry, Geophysics, Geosystems, v. 14, n. 3, p. 712–732, https://doi.org/10.1002/ggge.20068
Sparks, R. S. J., 1986, The role of crustal contamination in magma evolution through geological time: Earth and Planetary Science Letters, v. 78, n. 2–3, p. 211–223, https://doi.org/10.1016/0012-821X(86)90062-2
Tang, Q.-Y., Ma, Y.-S., Zhang, M.-J., Li, C., Zhu, D., and Tao, Y., 2013, The Origin of Ni-Cu-PGE Sulfide Mineralization in the Margin of the Zhubu Mafic-Ultramafic Intrusion in the Emeishan Large Igneous Province, Southwestern China: Economic Geology, v. 108, n. 8, p. 1889–1901, https://doi.org/10.2113/econgeo.108.8.1889
Tao, Y., Li, C., Hu, R.-Z., Ripley, E. M., Du, A.-D., and Zhong, H., 2007, Petrogenesis of the Pt–Pd mineralized Jinbaoshan ultramafic intrusion in the Permian Emeishan large igneous province, SW China: Contributions to Mineralogy and Petrology, v. 153, n. 3, p. 321–337, https://doi.org/10.1007/s00410-006-0149-5
Tao, Y., Ma, Y.-S., Miao, L.-C., and Zhu, F.-L., 2009, SHRIMP U-Pb zircon age of the Jinbaoshan ultramafic intrusion, Yunnan Province, SW China: Chinese Science Bulletin, v. 54, n. 1, p. 168–172, https://doi.org/10.1007/s11434-008-0488-x
Wang, C. Y., Zhou, M.-F., and Qi, L., 2007, Permian flood basalts and mafic intrusions in the Jinping (SW China)-Song Da (northern Vietnam) district: Mantle sources, crustal contamination and sulfide segregation: Chemical Geology, v. 243, n. 3–4, p. 317–343, https://doi.org/10.1016/j.chemgeo.2007.05.017
Wang, C. Y., Zhou, M.-F., and Zhao, D.-G., 2008, Fe-Ti-Cr oxides from the Permian Xinjie mafic-ultramafic layered intrusion in the Emeishan large igneous province, SW China: Crystallization from Fe-and Ti-rich basaltic magmas: Lithos, v. 102, n. 1–2, p. 198–217, https://doi.org/10.1016/j.lithos.2007.08.007
Wang, C. Y., Zhou, M.-F., Yang, S.-H., Qi, L., and Sun, Y.-L., 2014, Geochemistry of the Abulangdang intrusion: Cumulates of high-Ti picritic magmas in the Emeishan large igneous province, SW China: Chemical Geology, v. 378–379, p. 24–39, https://doi.org/10.1016/j.chemgeo.2014.04.010
Wendlandt, R. F., 1982, Sulfide saturation of basalt and andesite melts at high pressures and temperatures: American Mineralogist, v. 67, n. 9–10, p. 877–885.
Xiao, L., Xu, Y.-G., Mei, H.-J., Zheng, Y.-F., He, B., and Pirajno, F., 2004, Distinct mantle sources of low-Ti and high-Ti basalts from the western Emeishan large igneous province, SW China: Implications for plume-lithosphere interaction: Earth and Planetary Science Letters, v. 228, n. 3–4, p. 525–546, https://doi.org/10.1016/j.epsl.2004.10.002
Xu, Y.-G., Chung, S.-L., Jahn, B. M., and Wu, G., 2001, Petrologic and geochemical constraints on the petrogenesis of Permian-Triassic Emeishan flood basalts in southwestern China: Lithos, v. 58, n. 3–4, p. 145–168, https://doi.org/10.1016/S0024-4937(01)00055-X
Xu, Y.-G., He, B., Chung, S.-L., Menzies, M. A., and Frey, F. A., 2004, Geologic, geochemical, and geophysical consequences of plume involvement in the Emeishan flood-basalt province: Geology, v. 32, n. 10, p. 917–920, https://doi.org/10.1130/G20602.1
Xu, Y.-G., Luo, Z.-Y., Huang, X.-L., He, B., Xiao, L., Xie, L.-W., and Shi, Y.-R., 2008, Zircon U-Pb and Hf isotope constraints on crustal melting associated with the Emeishan mantle plume: Geochimica et Cosmochimica Acta, v. 72, n. 13, p. 3084–3104, https://doi.org/10.1016/j.gca.2008.04.019
Yu, S.-Y., Song, X.-Y., Chen, L.-M., and Li, X.-B., 2014, Postdated melting of subcontinental lithospheric mantle by the Emeishan mantle plume: Evidence from the Anyi intrusion, Yunnan, SW China: Ore Geology Reviews, v. 57, p. 560–573, https://doi.org/10.1016/j.oregeorev.2013.08.006
Yu, S.-Y., Song, X.-Y., Ripley, E. M., Li, C., Chen, L.-M., She, Y.-W., and Luan, Y., 2015, Integrated O–Sr–Nd isotope constraints on the evolution of four important Fe–Ti oxide ore–bearing mafic–ultramafic intrusions in the Emeishan large igneous province, SW China: Chemical Geology, v. 401, p. 28–42, https://doi.org/10.1016/j.chemgeo.2015.02.020
Zhang, X.-Q., Zhang, J.-F., Song, X.-Y., Deng, Y.-F., Guan, J.-X., Zheng, W.-Q., 2011, Implications of compositions of plagioclase and olivine on the formation of the Panzhihua V-Ti magnetite deposit, Sichuan Province: Acta Petrologica Sinica, v. 27, p. 3675–3688.
Zhang, X.-Q., Song, X.-Y., Chen, L.-M., Xie, W., Yu, S.-Y., Zheng, W.-Q., Deng, Y.-F., Zhang, J.-F., and Gui, S.-G., 2012, Fractional crystallization and the formation of thick Fe-Ti-V oxide layers in the Baima layered intrusion, SW China: Ore Geology Reviews, v. 49, p. 96–108, https://doi.org/10.1016/j.oregeorev.2012.09.003
Zhang, X.-Q., Song, X.-Y., Chen, L.-M., Yu, S.-Y., Xie, W., Deng, Y.-F., Zhang, J.-F., and Gui, S.-G., 2013, Chalcophile element geochemistry of the Baima layered intrusion, Emeishan Large Igneous Province, SW China: Implications for sulfur saturation history and genetic relationship with high-Ti basalts: Contributions to Mineralogy and Petrology, v. 166, n. 1, p. 193–209, https://doi.org/10.1007/s00410-013-0871-8
Zhang, Z.-C., Mahoney, J. J., Mao, J.-W., and Wang, F.-S., 2006, Geochemistry of picritic and associated basalt flows of the western Emeishan flood basalt province, China: Journal of Petrology, v. 47, n. 10, p. 1997–2019, https://doi.org/10.1093/petrology/egl034
Zhang, Z.-C., Mao, J.-W., Saunders, A. D., Ai, Y., Li, Y., and Zhao, L., 2009, Petrogenetic modeling of three mafic-ultramafic layered intrusions in the Emeishan large igneous province, SW China, based on isotopic and bulk chemical constraints: Lithos, v. 113, n. 3–4, p. 369–392, https://doi.org/10.1016/j.lithos.2009.04.023
Zhong, H., and Zhu, W.-G., 2006, Geochronology of layered mafic intrusions from the Pan-Xi area in the

Emeishan large igneous province, SW China: Mineralium Deposita, v. 41, n. 6, p. 599–606, https://doi.org/10.1007/s00126-006-0081-7

Zhong, H., Zhou, X.-H., Zhou, M.-F., Sun, M., and Liu, B.-G., 2002, Platinum-group element geochemistry of the Hongge Fe-V-Ti deposit in the Pan-Xi area, southwestern China: Mineralium Deposita, v. 37, n. 2, p. 226–239, https://doi.org/10.1007/s00126-001-0220-0

Zhong, H., Yao, Y., Prevec, S. A., Wilson, A. H., Viljoen, M. J., Viljoen, R. P., Liu B.-G., and Luo, Y.-N., 2004, Trace-element and Sr-Nd isotopic geochemistry of the PGE-bearing Xinjie layered intrusion in SW China: Chemical Geology, v. 203, n. 3–4, p. 237–252, https://doi.org/10.1016/j.chemgeo.2003.10.008

Zhong, H., Zhu, W.-G., Qi, L., Zhou, M.-F., Song, X.-Y., and Zhang, Y., 2006, Platinum-group element (PGE) geochemistry of the Emeishan basalts in the Pan-Xi area, SW China: Chinese Science Bulletin, v. 51, n. 7, p. 845–854, https://doi.org/10.1007/s11434-006-0845-6

Zhong, H., Qi, L., Hu, R.-Z., Zhou, M.-F., Gou, T.-Z., Zhu, W.-G., Liu, B.-G., and Chu, Z.-Y., 2011a, Rhenium-osmium isotope and platinum-group elements in the Xinjie layered intrusion, SW China: Implications for source mantle composition, mantle evolution, PGE fractionation and mineralization: Geochimica et Cosmochimica Acta, v. 75, n. 6, p. 1621–1641, https://doi.org/10.1016/j.gca.2011.01.009

Zhong, H., Campbell, I. H., Zhu, W.-G., Allen, C. M., Hu, R.-Z., Xie, L.-W., and He, D.-F., 2011b, Timing and source constraints on the relationship between mafic and felsic intrusions in the Emeishan large igneous province: Geochimica et Cosmochimica Acta, v. 75, n. 5, p. 1374–1395, https://doi.org/10.1016/j.gca.2010.12.016

Zhou, M.-F., Malpas, J., Song, X.-Y., Robinson, P. T., Sun, M., Kennedy, A. K., Lesher, C. M., and Keays, R. R., 2002, A temporal link between the Emeishan large igneous province (SW China) and the end-Guadeloupian mass extinction: Earth Planetary Science Letters, v. 196, n. 3–4, p. 113–122, https://doi.org/10.1016/S0012-821X(01)00608-2

Zhou, M.-F., Robinson, P. T., Lesher, C. M., Keays, R. R., Zhang, C. J., and Malpas, J., 2005, Geochemistry, petrogenesis and metallogenesis of the Panzhihua gabbroic layered intrusion and associated Fe-Ti-V oxide deposits, Sichuan Province, SW China: Journal of Petrology, v. 46, n. 11, p. 2253–2280, https://doi.org/10.1093/petrology/egi054

Zhou, M.-F., Arndt, N. T., Malpas, J., Wang, C. Y., and Kennedy, A. K., 2008, Two magma series and associated ore deposit types in the Permian Emeishan large igneous province, SW China: Lithos, v. 103, n. 3–4, p. 352–368, https://doi.org/10.1016/j.lithos.2007.10.006

Zhou, M.-F., Chen, W. T., Wang, C. Y., Prevec, S. A., Liu, P.-P., and Howarth, G. H., 2013, Two stages of immiscible liquid separation in the formation of Panzhihua-type Fe-Ti-V oxide deposits, SW China: Geoscience Frontiers, v. 4, n. 5, p. 481–502, https://doi.org/10.1016/j.gsf.2013.04.006

Zhu, W.-G., Zhong, H., Hu, R.-Z., Liu, B.-G., He, D.-F., Song, X.-Y., and Deng, H.-L., 2010, Platinum-group minerals and tellurides from the PGE-bearing Xinjie layered intrusion in the Emeishan Large Igneous Province, SW China: Mineralogy and Petrology, v. 98, n. 1, p. 167–180, https://doi.org/10.1007/s00710-009-0077-y